Phase Retrieval Using Complex Speckle Illumination Patterns and Multiplexing

Maxim Marshall

July 14, 2023

Bachelor Project

Supervisor: dr. Ksenia Abrashitova, dr. Tristan van Leeuwen

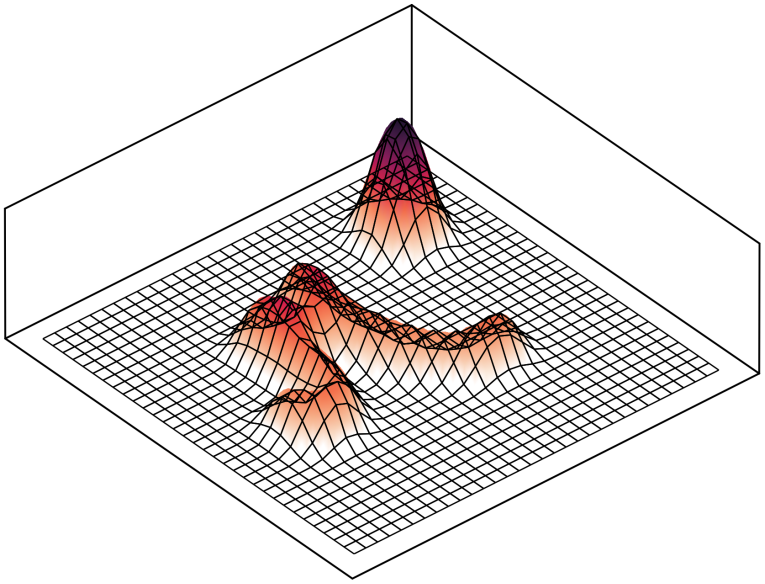

Advanced Research Center for Nanolithography

Faculty of Science

University of Amsterdam

Abstract

A method is proposed for reconstructing the phase of the optical response function of some object by illuminating the object with complex illumination patterns, and measuring the power and power spectral centroid position at the image plane for each pattern. The method is shown to work for complex speckle patterns as produced by a multi-mode waveguide. Alongside the continuous derivation of the method, a totally discrete analog is derived for use in numerical simulations. We also show that uniform random complex illumination patterns can be used instead of speckle patterns. The reconstructed optical response function differs from the ground truth by a factor of 10^{-11} in simulation, from which we claim that the reconstruction is exact.

Title: Phase Retrieval Using Complex Speckle Illumination Patterns and Multiplexing
Authors: Maxim Marshall, m@maximzuriel.nl, 13111531
Supervisor: dr. Ksenia Abrashitova, dr. Tristan van Leeuwen
Second grader: dr. Lyuba Amitonova
Date: July 14, 2023

Advanced Research Center for Nanolithography
Science Park 106, 1098 XG Amsterdam
`https://arcnl.nl/`

Samenvatting

Een camerabeeld bevat informatie over de helderheid van een object, ofwel de intensiteit van het licht dat door het object wordt gereflecteerd. Bijvoorbeeld, een appel op de grond is goed zichtbaar op een foto omdat de appel veel licht reflecteert. Zo'n foto is dus eigenlijk een meting van lichtintensiteit.

Licht heeft ook golfkenmerken, waardoor het in principe ook mogelijk zou moeten zijn om naast een intensiteitsbeeld ook een fasebeeld te maken. Een golf op zee ziet er anders uit afhankelijk van waar je schip zich bevindt, of met andere woorden, afhankelijk van wat de fase van de golf is. Helaas is de frequentie van licht erg hoog, waardoor de fase erg moeilijk te detecteren is. Wij bieden een methode aan om naast een intensiteitsbeeld ook een fasebeeld te maken. De toepassingen hiervan zijn breed.

Een aanzienlijk deel van het menselijk lichaam is doorzichtig, waardoor een intensiteitsbeeld niet veel informatie oplevert. Daaraantegen kan een fasebeeld veel betekenen voor een arts. De fase van licht wordt beïnvloed door de dichtheid en samenstelling van materialen, ook doorzichtige materialen.

Het maken van een fasebeeld wordt bereikt door het object te belichten met verschillende lichtpatronen. Vervolgens wordt een meting gedaan van de "gemiddelde ruimtelijke frequentie" van het object, zoals belicht door de patronen. De ruimtelijke frequentie is vergelijkbaar met de gebruikelijke frequentie zoals bij geluidsgolven, maar in plaats van een verandering in de tijd hebben we het hier over een verandering in de ruimte. We hebben een wiskundige relatie afgeleid waarmee deze metingen kunnen worden omgezet in een fasebeeld van het object.

De lichtpatronen worden gegenereerd door een laser op een fiber te richten, een soort doorzichtige draad waar het licht doorheen kan reizen. Het licht dat aan de andere kant uitkomt, is in feite willekeurig. Als de fiber een beetje wordt gebogen of bewogen, verandert het resulterende patroon. Hiermee kunnen er op een goedkope en snelle manier veel lichtpatronen worden gegenereerd.

Daarnaast hebben we ook een methode bedacht waarmee je dit alles kunt simuleren op de computer. Onze numerieke simulatieaanpak resulteert in een verschil tussen de invoer en uitvoer van de simulatie van de orde van 10^{-11}. Dit is een enorme verbetering in vergelijking met een verschil van 10^{-1} bij het gebruiken van voor de hand liggende simulatietechnieken.

Contents

1. Introduction **6**

2. Method and Theory **8**
2.1. Method 8
2.2. Theory 11
2.2.1. Multiplexing with Complex Weights 13
2.2.2. Amplitude Reconstruction by Means of Multiplexing 14
2.2.3. Phase Reconstruction by Means of Multiplexing 15
2.2.4. Special Cases of the Continuous Equation 17
2.2.5. Considerations for Measurement Sensitivity 18
2.3. Exact Discrete Analysis 21
2.3.1. Discretization of the Continuous Result 22
2.3.2. Matrix Form Representation 26
2.3.3. Numerical Simulation of Phase Reconstruction 28
2.4. Scheme for Reconstructing Phase from Measurements 30

3. Results **34**
3.1. Uniform Random Complex Illumination Patterns 34
3.2. Artificial Complex Speckle Illumination Patterns 37
3.2.1. Dependence of Reconstruction on Algorithm Parameters 37
3.3. Comparison with Previous Approach 41
3.4. Experimentally Obtained Complex Speckle Illumination Patterns 44

4. Discussion **46**

5. Conclusion **47**

6. Acknowledgements **48**
6.1. Software and Tooling 48

7. Bibliography **49**

A. Proofs **51**
A.1. Fourier Transform Theorems 51
A.2. Derivation of Continuous Equation 52
A.3. Derivation of Discrete Equation 52

B. Algorithms **54**
B.1. Construction of Artificial Speckle Patterns 55

1. Introduction

The problem of reconstructing the phase of a signal from intensity measurements of the modulus of its Fourier transform is of interest to many areas of engineering and applied physics, and has gained due attention [1, 2, 3, 4]. In optics, it is often the case that the phase of a signal contains more information about the imaged object than the signal intensity [5]. In astronomy, a solution to the phase retrieval problem allows reconstruction of images from intensity interferometry data [6]. Likewise and among others, the fields of computational biology, X-ray crystallography, blind deconvolution and speech processing, all have something to gain from a solution to the phase retrieval problem [2].

In optics, the electric field after having interacted with a physical object can be described using the Optical Response Function (ORF) of that object, $\gamma(x, y) = t(x, y)e^{\mathrm{i}\varphi(x,y)}$. If we illuminate the object with a monochromatic and linearly polarized plane wave, then the amplitude $t(x, y)$ represents how much of the light is reflected and ranges from 0 to 1, and the phase $\varphi(x, y)$ represents the retardation of the electromagnetic wavefront at each point.

The wavefront is thus assumed to have passed through, or otherwise have interacted with a physical object, such that information about the object of interest is contained in the wavefront. Intensity measurements as taken by an ordinary camera will contain information about the ORF amplitude $t(x, y)$. But as an artefact of the fast oscillatory nature of the signal, being that it represents a wavefront of light, the detector necessarily integrates many periods of the signal during each measurement. Information about the phase $\varphi(x, y)$ is then lost in the process.

From Fraunhofer diffraction theory we know that the electromagnetic field at the object plane, say E^{obj}, transforms to the field at the image plane according to $E^{\mathrm{out}}(u, v) = \mathfrak{F}\{E^{\mathrm{obj}}(x, y)\}/\mathrm{i}\lambda f$, where $\mathfrak{F}\{.\}$ denotes the Fourier transform [7]. Here, x, y are the coordinates of the object plane, and u, v are the coordinates of the image plane. We show that by illuminating the object with a series of alternating illumination patterns which are assumed to be known *a priory*, it is possible to exactly reconstruct γ in both amplitude t and phase φ from intensity measurements alone. More so, the scheme we will

describe requires but a quadrant detector at the image plane, as opposed to a camera.

Methods exist for solving the phase retrieval problem as defined here, but additional assumptions on the experimental setup, such as the availability of interferometry [8], or additional knowledge of the object [9], result in restricted practical applications. The proposed method tackles the case of illumination that is not entirely controlled, in that the phase and amplitude of the illumination are both somewhat arbitrary. We assume that such a setup would allow for calibration, such that the illumination patterns, although arbitrary, could be reproduced after calibration. A specific example satisfying this description is coherent monochromatic light that passes through a multi-mode fiber and gets scrambled into a speckle pattern in the process.

A related avenue was explored in previous works, and is referred to as spatial sampling, but an additional restriction of illumination that is constant in phase makes this approach expensive to implement in an experimental setting [10, 1]. We instead derive a multiplexing scheme that allows for the recovery of both phase and amplitude of the ORF using complex illumination patterns for the multiplexing weights. The method is shown to work for arbitrary signals and for illumination patterns representative of speckle patterns as produced by multi-mode fibers. A totally discrete relation for use in computer simulations is additionally derived, with which the difference between the reconstructed signal and the ground truth is of the order of 10^{-11}, as opposed to a difference of the order of 10^{-1} which we obtained using the method described in [11].

The relations and their full derivations, and the relevant background theory will be presented in chapter 2, alongside the methods and algorithms used to test the derived relations numerically. The results will be presented and analyzed in chapter 3, and discussed in chapter 4. Concluding remarks will be given in chapter 5. Some proofs were delegated to appendix A. Auxiliary algorithms used to implement the computer simulations can be found in appendix B.

2. Method and Theory

The magnitude of the Fourier transform of a signal is related to both the phase and amplitude of the signal; this relationship allows for the recovery of the complex signal from intensity measurements alone, intensity being the square of the magnitude. The Fourier transform of a function $f(t)$ is written as $\hat{f}(\omega) = \mathfrak{F}\{f(t)\}$ and is given by

$$\mathfrak{F}\{f(t)\}(\omega) \coloneqq \int_{-\infty}^{\infty} f(t)e^{-2\pi i\omega t}\,dt, \quad t, \omega \in \mathbb{R}^n. \tag{2.1}$$

Obtaining the Fourier transformed signal is easily done experimentally if the signal represents an electromagnetic wavefront, as is the case in optics.

2.1. Method

Consider a linearly polarized monochromatic plane wave that hits a planar transparency at normal incidence, which we will call the object, having amplitude transmittance $t(x, y)$. Let the change of phase of the plane wave due to the transparency in addition to the change in amplitude be represented by the Optical Response Function (ORF) of the object

$$\gamma(x, y) = t(x, y)e^{\mathrm{i}\varphi(x,y)}. \tag{2.2}$$

Here, the amplitude transmittance $t(x, y)$ ranges from 0 to 1, and $\varphi(x, y)$ is the phase of the wavefront after interacting with the transparency. Let $E^{\mathrm{obj}}(x, y)$ be the field immediately adjacent to the plane of the transparency, the object plane. An intensity measurement of the object field would yield $\left|E^{\mathrm{obj}}(x, y)\right|^2$, as is the case with an ordinary camera. However, the phase information $\varphi(x, y)$ is lost during measurement. It is the purpose of this method to reconstruct the lost phase information.

When a field $E^{\mathrm{obj}}(x, y)$ at the object plane passes through a converging lens, placed equally far from the object plane as from the image plane at the focal distance f, the field at the image plane $E^{\mathrm{out}}(u, v)$ is exactly equal to the Fourier transform of the field at the object plane [7]

$$E^{\text{out}}(u,v) = \frac{1}{\mathrm{i}\lambda f}\mathfrak{F}(\omega_x,\omega_y)\{E^{\text{obj}}(x,y)\}. \tag{2.3}$$

Here, x, y are the coordinates in the object plane, u, v are the coordinates in the image plane, and λ is the wavelength of the monochromatic illumination. Thus, the amplitude and phase of the field at the image plane at the coordinates (u,v) is entirely determined by the amplitude and phase of the Fourier component of the field at the object plane, concerning the spatial frequencies $\omega_x = u/\lambda f$ and $\omega_y = v/\lambda f$ specifically [7]. The object can be taken to be, for the sake of naming a concrete example, a transparent biological sample to be imaged. Since light travels at different speeds through different media, the wavefront will deform according to the geometry, density and composition of the physical object.

There exist methods which make use of this Fourier transform relationship to reconstruct the object, both the intensity field and phase, from intensity measurements alone; two of which being Shack-Hartmann sensors and spatial wavefront sampling [11]. Shack-Hartmann sensors consist of an array of small lenses, each of which produces a focal spot on the detector, the displacement of which corresponding to the local slope of the wavefront of the object (fig. 2.1 a). The resolution of these sensors is dependant on the number of lenses one can fit in the sensor, making them expensive and challenging to manufacture.

The second mentioned method, spatial wavefront sampling, side-steps this limitation by multiplexing the measurements. Instead of an array of lenses, a single lens along with a series of masks are used to collect a series of measurements, each measurement sampling different portions of the object simultaneously (fig. 2.1 b). The signal is then reconstructed by demultiplexing the measurements [11]. These masks can be troublesome to manufacture, but alternatively one can spatially sample the object by selectively illuminating it, eliminating the need for masks. This however requires the illumination to have constant phase, as is not typically the case. In other words, the illumination must be a plane wave. Such a light source might not always be practical, if available at all.

The approach taken in this thesis derives from spatial wavefront sampling, but extends the method to allow for illumination patterns of varying amplitude and phase, thereby easing the requirements on the illumination patterns (fig. 2.1 c). This method is shown to work for uniformly distributed random complex illumination patterns, computer generated complex speckle patterns, and for complex speckle patterns produced by the output of a multi-mode fiber.

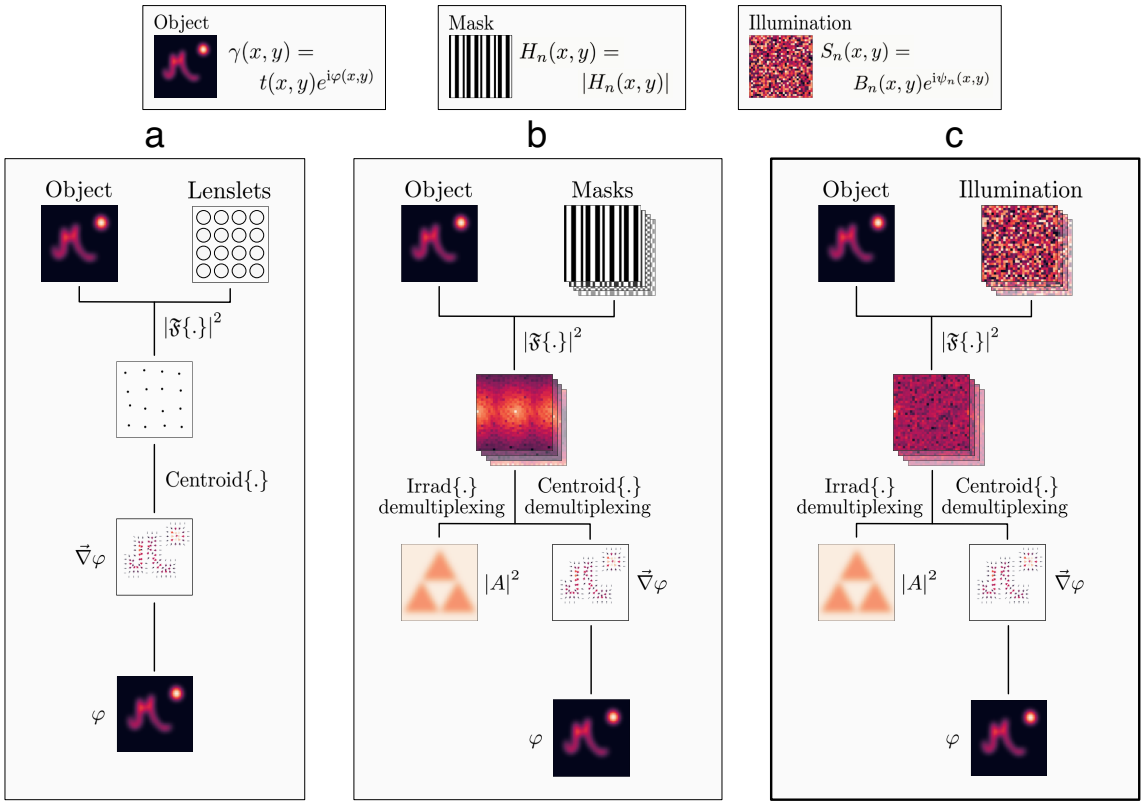

Figure 2.1.: Three approaches for the phase retrieval problem, the first two (a, b) are adapted from [11], the proposed method (c) is presented last. (a) An object is imaged through a lenslet array. Each lenslet produces a focal spot on the detector, the position of which contains information about the phase gradient of the object. (b) An object is sequentially illuminated by a series of binary patterns, that is to say, only some parts of the object plane are illuminated at each measurement. The total irradiance and centroid position of each measurement are used to reconstruct the amplitude and phase gradient of the object, respectively, by means of demultiplexing. The phase is then obtained by numerical integration. (c) The proposed approach; an object is sequentially illuminated by a set of complex illumination patterns. The resulting measurements are then demultiplexed according to the theory that is worked out throughout the body of this thesis.

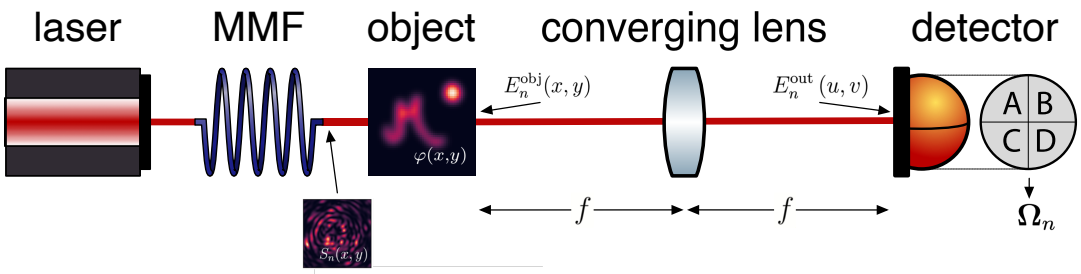

Figure 2.2.: A monochromatic laser of wavelength λ illuminates one end of a multi-mode fiber (MMF); the light that exits (referred to by $S_n(x,y)$, only $|S_n|^2$ is depicted) is scrambled into a certain speckle pattern. This light is used to illuminate an object, which has as its ORF the function $\gamma(x,y) = t(x,y)e^{\mathrm{i}\varphi(x,y)}$. The resulting field is referred to by $E_n^{\text{obj}}(x,y)$ for the nth speckle pattern. This field passes through a converging lens placed equally far from the detector and the object at a distance equal to the focal length of the lens, f. The detector is a quadrant field detector, it measures the total power P_n and the power spectral centroid position $\mathbf{\Omega}_n$ of the field $E_n^{\text{out}}(u,v)$. Note that x, y are the coordinates of the object plane, and u, v are the coordinates of the image plane. Both range from $-\infty$ to ∞ and are centered with respect to the optical axis.

2.2. Theory

We wish to reconstruct the complex object field $E^{\text{obj}}(x,y)$ from intensity measurements alone. To do this, we make use of Fraunhofer diffraction theory, which states that a converging lens with focal length f placed between the object and the detector a distance f apart from each, results in a reading of the Fourier transform of the object field at the detector (fig. 2.3) [7]. The field at the object plane transforms to the field at the detector plane according to eq. (2.3), giving a direct relationship between the field at the image plane and the Fourier transform of the field at the object plane.

To better understand this relationship, one can note that if the object field is masked by a small square field-stop, then the power P and the power spectral centroid position $\mathbf{\Omega}$ relate to the intensity of the object field $\left|E^{\text{obj}}(x,y)\right|^2$ and its phase gradient $\boldsymbol{\nabla}\varphi(x,y)$, respectively, at the position of the field-stop [11]. Alternatively, instead of using a field-stop, one can illuminate only the part of the object of which the field would pass through the field-stop, were it to be there. For this alternative representation to hold, the illumination must be constant in intensity and phase. We will extend this relationship

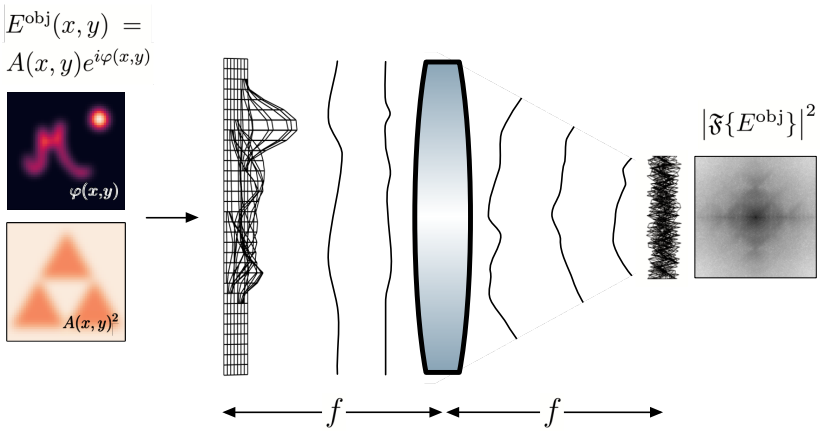

Figure 2.3.: A converging lens placed halfway between the photo subject and the detector, a distance of the focal length apart from each, will act as a Fourier transform on the object field. The object field is shown both in amplitude and phase (left), and the field at the detector (right) is shown in the logarithm of the intensity. Additionally, the deformation of the wavefronts as described by the phase are illustrated at intermediary points.

to relate P and $\mathbf{\Omega}$ to $\left|E^{\text{obj}}(x,y)\right|^2$ and $\boldsymbol{\nabla}\varphi(x,y)$, respectively, for the most general form of illumination, namely illumination that varies in intensity and phase.

With that extension, we show that by illuminating the object with patterns of varying phase and intensity, and measuring the intensity of the field at the image plane for each pattern, we can recover the object field by demultiplexing the measurements. From eq. (2.3) it is evident that the power spectrum of the object field is obtained by taking the intensity of the field at the image plane. The method requires only knowledge of the power of the field at the image plane, and the centroid position of the intensity of that field, which we will denote as P_n and $\mathbf{\Omega}_n$ respectively for the nth illumination pattern. This significantly simplifies measurements by removing the requirement for a camera, instead requiring only four electrodes at the image plane [11].

Throughout this derivation, when we talk of measured fields or fields that are used in computer simulations, we implicitly assume uniform sampling. That is, the measured fields are assumed to be the average of the field over the resolution elements of a hypothetical detector

$$E[x',y'] = \frac{1}{\epsilon^2}\int_{x'\epsilon-\epsilon/2}^{x'\epsilon+\epsilon/2}\int_{y'\epsilon-\epsilon/2}^{y'\epsilon+\epsilon/2} E(x,y)\,dx\,dy. \tag{2.4}$$

The variables x' and y' represent a resolution element of the detector, and range from 1 to W, and 1 to H respectively, if the detector is of resolution $W \times H$. Additionally, ϵ represents the width of each of the assumed square resolution elements. Square brackets were introduced to emphasize that the measured field is necessarily discrete.

2.2.1. Multiplexing with Complex Weights

By sampling the object field spatially at multiple points simultaneously, we can reconstruct the field using but one quadrant detector, as opposed to a detector of many resolution elements. The operational principle is that by weighting each point by some function, and measuring the weighted sum for a well-formed set of weighting functions, we essentially measure the projection of the field along the basis formed by those functions. The sense in which the set of functions must be well-formed will be explained momentarily. This process is called multiplexing and it works as follows.

Suppose we have a way of weighting some function $f(x, y)$ by another function $S_n(x, y)$, such that the signal at the nth measurement is given by $f_n(x, y) = f(x, y)S_n(x, y)$. Suppose also that we can measure the integrated signal, that is, $\iint f_n(x, y)\, dx\, dy$. Here and from here on forth, all integrals are to be taken over the range $(-\infty, \infty)$ unless otherwise stated.

If for the sake of brevity we sample the functions uniformly on a 2×2 grid, we can see that four measurements are enough to reconstruct $f(x, y)$ exactly. Each measurement, say η_n, can be written as a sum over the sampling grid coordinates

$$\iint f_n(x, y)\, dx\, dy \longrightarrow \sum_{x' \in \{0,1\}} \sum_{y' \in \{0,1\}} f_n[x', y'], \tag{2.5}$$

where x', y' represent the coordinates on the sampling grid and x, y represent continuous coordinates. If N measurements are taken, then we can write each measurement as the product of a row matrix corresponding to the sampled weighting function $S_n[x', y']$, and a column matrix corresponding to the sampled signal $f[x', y']$

$$\begin{pmatrix} S_0[0,0] & S_0[1,0] & S_0[0,1] & S_0[1,1] \\ S_1[0,0] & S_1[1,0] & S_1[0,1] & S_1[1,1] \\ \vdots & \vdots & \vdots & \vdots \\ S_{N-1}[0,0] & S_{N-1}[1,0] & S_{N-1}[0,1] & S_{N-1}[1,1] \end{pmatrix} \begin{pmatrix} f[0,0] \\ f[1,0] \\ f[0,1] \\ f[1,1] \end{pmatrix} = \begin{pmatrix} \eta_0 \\ \eta_1 \\ \vdots \\ \eta_{N-1} \end{pmatrix}. \tag{2.6}$$

The fields were flattened so that they can be written as vectors. That is just a shift of representation and it bares no physical significance.

It is evident that in this case, four measurements are required for eq. (2.6) to form a complete set of linear equations. But for a signal sampled such as to contain N values, N^2 measurements are required; although use of compressive sensing can significantly lower the required number of measurements [12]. The signal of interest $f(x, y)$ is then obtained from measurements by inverting eq. (2.6) and unwrapping the result. In order for this to be possible, the set of weighting functions must be chosen such that the matrix that they form, on the left hand side of eq. (2.6), is full rank [1].

If the optical response function of the object of interest is given by eq. (2.2), where the amplitude transmittance $t(x, y)$ ranges from 0 to 1, then the weighting scheme can be implemented by a modulated monochromatic light-source. The light-source will produce varying complex patterns, which we will refer to as illumination patterns. Let the field of the nth illumination pattern generated by this monochromatic light source as it arrives at the object plane be given by

$$S_n(x, y) = B_n(x, y)e^{\mathrm{i}\psi_n(x,y)}, \tag{2.7}$$

where $B_n(x, y)$ is the amplitude of the field, which can take an arbitrary but positive and real value, and $\psi_n(x, y)$ is the phase of the wavefront. This wavefront interacts with the object to form the field at the object plane,

$$E_n^{\mathrm{obj}}(x, y) = \gamma(x, y)S_n(x, y) = t(x, y)B_n(x, y)e^{\mathrm{i}(\varphi(x,y)+\psi_n(x,y))}. \tag{2.8}$$

With this we have the mechanism by which to implement the multiplexing scheme, namely by modulating the illumination of the object. The reconstruction of the phase $\varphi(x, y)$ is more involved than the reconstruction of the amplitude $t(x, y)$, so we will begin with the latter.

2.2.2. Amplitude Reconstruction by Means of Multiplexing

Consider the optical system shown in fig. 2.2, where a converging lens is placed equidistant and a focal length apart from the detector and the object, that is itself illuminated by the predetermined complex illumination patterns $S_n(x, y)$. The illumination is monochromatic and of wavelength λ; the distance between the lens and either the object or detector, the focal distance, is given by f. In this setup, the wavefront at the object plane $E_n^{\mathrm{obj}}(x, y)$ propagates towards the detector such that at the image plane, the wavefront $E_n^{\mathrm{out}}(u, v)$ is given by eq. (2.3).

The reconstruction of the amplitude $t(x, y)$ is particularly simple, since the field at the image plane is essentially the Fourier transform of the field at the object plane.

Theorem 2.2.1 (Plancherel's Theorem)**.** *If $f_1(t)$ and $f_2(t)$ are two $L^2(\mathbb{R}^n)$ functions, then*

$$\int_{-\infty}^{\infty} f_1(t) f_2(t)^* \, dt = \int_{-\infty}^{\infty} \hat{f}_1(\omega)(\hat{f}_2(\omega))^* \, d\omega, \quad t, \omega \in \mathbb{R}^n, \tag{2.9}$$

where the star denotes the complex conjugate and the hat denotes the Fourier transform.

From theorem 2.2.1 it follows that

$$\iint \left| E_n^{\text{obj}}(x, y) \right|^2 dx \, dy = \iint \left| E_n^{\text{out}}(u, v) \right|^2 du \, dv, \tag{2.10}$$

where x, y are the coordinates in the object plane, and u, v are the coordinates in the image plane. If we define

$$P_n = \iint \left| E_n^{\text{out}}(u, v) \right|^2 du \, dv \tag{2.11}$$

as the power (integrated intensity) of the field at the image plane, then we can additionally use eq. (2.7) and eq. (2.8) to write eq. (2.10) as

$$\boxed{P_n = \iint B_n(x, y)^2 t(x, y)^2 \, dx \, dy.} \tag{2.12}$$

The reconstruction of $t(x, y)$ then takes place by inverting eq. (2.6) as described in section 2.2.1, with the substitutions $f \leftarrow t^2$, $S_n \leftarrow B_n^2$, and $\eta_n \leftarrow P_n$, and taking the square root of the result. There is no ambiguity in the last step as $t(x, y)$ ranges from 0 to 1, by definition. A procedure for reconstructing the intensity from power measurements is provided in algorithm 3.

2.2.3. Phase Reconstruction by Means of Multiplexing

Reconstructing the phase $\varphi(x, y)$ is more involved, because there is no ready equation to relate the measurements to the field at the object plane. Nonetheless, we have derived such a relation. This relation will form the basis for the phase reconstruction, and we will provide it here with the proof delegated to appendix A.2.

Theorem 2.2.2. *If a complex analytic signal $f(t)$ vanishes at infinity, then*

$$\int |f(t)|^2 \nabla \arg(f(t)) \, dt = 2\pi \int \omega \left| \hat{f}(\omega) \right|^2 d\omega, \quad t, \omega \in \mathbb{R}^n \tag{2.13}$$

where $\hat{f}(\omega)$ is the Fourier transform of $f(t)$, and $\nabla \arg(f(t))$ is the gradient of the phase of $f(t)$.

We can substitute $E_n^{\text{obj}}(x,y)$ in theorem 2.2.2 to produce a key result of this derivation, a relation between the centroid position of $\left|E_n^{\text{out}}(u,v)\right|^2$ and the phase gradient of $E_n^{\text{obj}}(x,y)$,

$$\begin{aligned}\frac{2\pi}{\lambda f}\iint \begin{pmatrix} u \\ v \end{pmatrix} \cdot \left|E_n^{\text{out}}\,(u,v)\right|^2 du\,dv \\ = \iint \left|E_n^{\text{obj}}(x,y)\right|^2 \boldsymbol{\nabla}\left(\varphi(x,y)+\psi_n(x,y)\right)\,dx\,dy.\end{aligned} \tag{2.14}$$

Here, x, y are the coordinates in the object plane, u, v are the coordinates in the image plane, λ is the wavelength of the illumination, f is the focal distance, $\psi_n(x,y)$ is the phase of the nth illumination pattern and $\varphi(x,y)$ is the phase of the object ORF.

The left hand side of eq. (2.14) corresponds to the spectral power centroid of the object field, a measurable quantity that is given by

$$\boldsymbol{\Omega}_n = \begin{pmatrix} \Omega_n^u \\ \Omega_n^v \end{pmatrix} = \frac{1}{P_n}\iint \begin{pmatrix} u \\ v \end{pmatrix} \cdot \left|E_n^{\text{out}}(u,v)\right|^2 du\,dv, \tag{2.15}$$

with $P_n = \iint \left|E_n^{\text{out}}(u,v)\right|^2 du\,dv$ being the power (integrated intensity) of the field at the image plane, which by theorem 2.2.1 we know also equals $P_n = \iint \left|E_n^{\text{obj}}(x,y)\right|^2 dx\,dy$. The right hand side of eq. (2.14) consists of the phase gradient of the object ORF, the assumed known phase gradient of the illumination pattern, and the obtainable intensity of the field at the object plane.

The object field intensity is obtainable from ordinary intensity measurements, so the second term of the right hand side of eq. (2.14) is a known constant for each measurement. We use eq. (2.8) to write this constant term as

$$\boldsymbol{C}_n = \frac{\lambda f}{2\pi P_n}\iint t(x,y)^2 B_n(x,y)^2\,\boldsymbol{\nabla}\psi_n(x,y)\,dx\,dy. \tag{2.16}$$

Using these definitions and eq. (2.8), eq. (2.14) can be written explicitly in terms of the measurable and known quantities, and the unknown phase gradient of the object ORF

$$\boxed{\boldsymbol{\Omega}_n = \frac{\lambda f}{2\pi P_n}\iint t(x,y)^2 B_n(x,y)^2\,\boldsymbol{\nabla}\varphi(x,y)\,dx\,dy + \boldsymbol{C}_n,} \tag{2.17}$$

where $\boldsymbol{\nabla}\varphi(x,y)$ is the phase gradient of the object ORF, $t(x,y)$ is the amplitude of the object ORF, $B_n(x,y)^2$ is the intensity of the nth illumination pattern, $\boldsymbol{\Omega}_n$ is a measurable quantity that corresponds to the power spectral centroid of the object field, P_n is the

total power of the field at the image plane, $\boldsymbol{C}_n$ is a constant determined by the nth illumination pattern, λ is the wavelength of the illumination and f is the focal length.

This is the main result of this thesis; using this relation, the phase gradient of the object ORF $\boldsymbol{\nabla}\varphi(x, y)$ can be obtained in a similar manner to section 2.2.2. The only restrictions on eq. (2.17) are that the fields vanish at infinity, and that if they are sampled, that they are sampled below the Nyquist frequency.

Since we also know how to reconstruct the object ORF amplitude $t(x, y)$ (section 2.2.2), and the phase $\varphi(x, y)$ is trivially obtained by numerical integration of the phase gradient, we hereby have a method to exactly reconstruct the object ORF $\gamma(x, y)$ from intensity measurements alone. The reconstruction of $\varphi(x, y)$ takes place by inverting eq. (2.6) as described in section 2.2.1, with the substitutions $f \leftarrow \nabla_x\varphi$, $S_n \leftarrow \lambda f \left|E_n^{\text{obj}}\right|^2/2\pi P_n$, and $\eta_n \leftarrow (\Omega_n)_x - (C_n)_x$ (*idem ditto* for y) and integrating the resulting phase gradient. We outline a procedure for reconstructing the object ORF from total power and power spectral centroid measurements in algorithm 4.

2.2.4. Special Cases of the Continuous Equation

It is worth mentioning a few special cases of eq. (2.14). If one considers a pure phase object, that is, an object that only influences the phase of the wavefront of the light illuminating it and not the intensity, then eq. (2.14) simplifies significantly. Such an object could for example be a transparent material, such as a magnifying glass, or a drinking glass.

We will now present eq. (2.14) as simplified in accordance to three special cases, all regarding a pure phase object: the first case assumes only a pure phase object, the second case additionally assumes that the phase of the illumination remains constant, and the third case assumes binary illumination. That is, an illumination pattern that consists only of entirely illuminating and entirely non-illuminating parts.

Complex Illumination of a Pure Phase Object

If the illumination patterns $S_n(x, y)$ are complex-valued, and the object ORF is of constant amplitude t, then

$$\boldsymbol{\Omega}_n = \frac{\lambda f t^2}{2\pi P_n} \iint |S_n(x, y)|^2 \, \boldsymbol{\nabla} \left(\varphi(x, y) + \psi_n(x, y)\right) \, dx \, dy, \quad S_n(x, y) \in \mathbb{C}^2 \tag{2.18}$$

where $\boldsymbol{\Omega}_n$ is the nth measurement of the power spectral centroid position, $\boldsymbol{\nabla}\varphi(x, y)$ is the phase gradient of the object ORF, P_n is the field power, λ is the wavelength, f is the focal distance, and $S_n(x, y)$ is the nth illumination pattern.

Real-Valued Illumination of a Pure Phase Object

If the illumination patterns $S_n(x, y)$ are real-valued, and the object ORF is of constant amplitude t, then

$$\mathbf{\Omega}_n = \frac{\lambda f t^2}{2\pi P_n} \iint S_n(x,y)^2 \, \boldsymbol{\nabla}\varphi(x,y) \, dx \, dy, \quad S_n(x,y) \in \mathbb{R}^2 \tag{2.19}$$

where $\mathbf{\Omega}_n$ is the nth measurement of the power spectral centroid position, $\boldsymbol{\nabla}\varphi$ is the phase gradient of the object ORF, P_n is the field power, λ is the wavelength, f is the focal distance, and $S_n(x, y)$ is the nth illumination pattern.

Binary Illumination of a Pure Phase Object

If the illumination patterns $S_n(x, y)$ are binary and thus consist only of either fully illuminating regions of constant phase, or non-illuminating regions, and the object ORF is of constant amplitude, then

$$\mathbf{\Omega}_n = \frac{\lambda f}{2\pi a_n} \iint_{\mathcal{A}_n} \boldsymbol{\nabla}\varphi(x,y) \, dx \, dy, \quad \text{(binary illumination)} \tag{2.20}$$

where $\mathbf{\Omega}_n$ is the nth measurement of the power spectral centroid position, $\boldsymbol{\nabla}\varphi(x, y)$ is the phase gradient of the object ORF, λ is the wavelength, f is the focal distance, $\mathcal{A}_n$ is the region of the object plane where the nth illumination pattern is non-zero, and $a_n = \iint_{\mathcal{A}_n} dx \, dy$ is the area corresponding to that region. This result is identical to that obtained in [11].

2.2.5. Considerations for Measurement Sensitivity

It is possible to qualitatively predict the power spectral centroid position $\mathbf{\Omega}_n$ for a given object and illumination pattern, something that is of interest for the experimental setup. When the object field has a large amplitude at the places where its phase gradient is slowly changing, the centroid position offset will be most pronounced. That much is evident by inspection of eq. (2.17). Indeed, the largest centroid position offset is obtained for pure phase objects of constant phase gradient.

Suppose that we illuminate a square pure phase object of length L with a plane wave of constant intensity I_{illum} and phase $\psi(x, y)$. Let the ORF of this object be given by the following function

$$U(x,y) = te^{2\pi \mathrm{i} g x}, \tag{2.21}$$

where x and y range from $-L/2$ to $L/2$, t is a constant real number between 0 and 1, and g is a real parameter that controls the rate of change of the phase of the object ORF. We can use eq. (2.18) to evaluate the centroid position

$$\boldsymbol{\Omega} = \frac{\lambda f t^2}{2\pi P} \iint_{-L/2}^{L/2} I_{\text{illum}} \boldsymbol{\nabla} \left(\varphi(x,y) + \psi(x,y)\right) \, dx \, dy \tag{2.22}$$

$$= \frac{\lambda f t^2 I_{\text{illum}}}{2\pi P} \left(\iint_{-L/2}^{L/2} \boldsymbol{\nabla} \left[2\pi g x\right] \, dx \, dy + \iint_{-L/2}^{L/2} \boldsymbol{\nabla} \psi(x,y) \, dx \, dy \right) \tag{2.23}$$

$$= \frac{\lambda f t^2 I_{\text{illum}}}{2\pi P} \left(\begin{pmatrix} 2\pi g L^2 \\ 0 \end{pmatrix} + \iint_{-L/2}^{L/2} \boldsymbol{\nabla} \psi(x,y) \, dx \, dy \right) \tag{2.24}$$

$$= \lambda f \left(g\hat{\boldsymbol{u}} + \frac{1}{2\pi L^2} \iint_{-L/2}^{L/2} \boldsymbol{\nabla} \psi(x,y) \, dx \, dy \right), \tag{2.25}$$

where the intensity of the object field was dropped against the power, as the former is constant, and where $\hat{\boldsymbol{u}}$ is the unit vector along the u-axis (the coordinates at the image plane are (u,v) and at the object plane (x,y)).

If we further assume plane wave illumination, then $\boldsymbol{\nabla}\psi_n(x,y)$ will vanish and we get the following expression for the centroid position

$$\boldsymbol{\Omega} = \lambda f g \hat{\boldsymbol{u}}. \tag{2.26}$$

We see that the centroid position depends linearly on the wavelength λ and focal distance f. Since the spatial frequency along the y-direction is zero, the centroid position along the v-direction is also zero. The centroid position along the u-direction depends linearly on the rate of change parameter g, such that a rapidly varying phase with respect to the x-direction will produce the largest centroid position offset.

If we take the wavelength to be 620 nm, which corresponds to red light, and we take the focal distance to be 100 mm, then we can inquire as to what value g must take for the centroid position offset to be measurable. Suppose that we can measure an offset of 4 mm, then we have as a lower bound $g > 6.5 \times 10^4 \, \text{m}^{-1}$. A simulation of this exact scenario is shown in fig. 2.4.

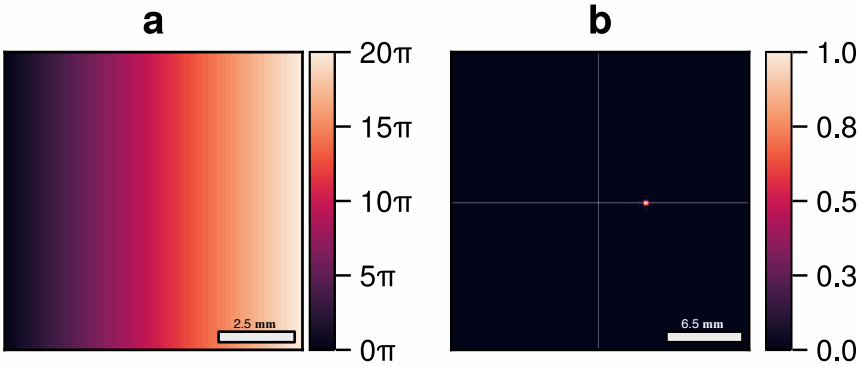

Figure 2.4.: The phase distribution of a pure phase object (a) is shown alongside the intensity distribution at the image plane due to that object (b). The portion of the object plane that is shown is a square of length 10 mm. The portion of the image plane that is shown is a square of length 26 mm. The power spectral centroid position offset is clearly readable, and it equals 4 mm. The simulation assumed plane wave illumination of constant intensity and a wavelength of 620 nm. The focal distance is 100 mm.

2.3. Exact Discrete Analysis

While it is at this point seemingly possible to test the method using computer simulations, we note that the naive discretization of eq. (2.14) results in a discrete equation that is sensitive to the smoothness of the signals. If one simply replaces the Fourier transform with the discrete Fourier transform (DFT), and the integrals with sums, then the relations will only hold for signals that are sampled at a sufficiently high rate, and only approximately at that. Specifically, the signals must be sampled below the Nyquist frequency. This translates to using a detector with a sufficiently high number of resolution elements. We give the naive discrete analog of eq. (2.14) for completeness

$$\begin{aligned} \frac{2\pi}{\lambda f W H} \sum_{u'=0}^{W-1} \sum_{v'=0}^{H-1} \begin{pmatrix} u' - W/2 \\ v' - H/2 \end{pmatrix} \cdot \left| E_n^{\text{out}}[u', v'] \right|^2 \\ \approx \sum_{x'=0}^{W-1} \sum_{y'=0}^{H-1} \left| E_n^{\text{obj}}[x', y'] \right|^2 \boldsymbol{\nabla} \left(\varphi[x', y'] + \psi_n[x', y'] \right). \end{aligned} \tag{2.27}$$

We assumed uniform sampling of the fields according to eq. (2.4), such that they are sampled on a $W \times H$ grid, where u', v' are the grid coordinates of the image plane and x', y' are the grid coordinates of the object plane.

The purpose of this section is to derive an entirely discrete, exact representation of eq. (2.17), such that the method can be tested with arbitrary signals. Although the requirement of using signals that vanish at infinity remains. The result is a relation analogous to the continuous one, in that it relates the phase gradient (backward difference) of a signal to the magnitude of its DFT, but this relation is not sensitive to the sampling rate.

Consider a signal $E(x, y)$ that is uniformly sampled on a $W \times H$ grid, to produce the discrete signal $E[x', y']$, as described by eq. (2.4). Here, x' ranges from 0 to $W - 1$ and y' ranges from 0 to $H - 1$. The discrete signal $E[x', y']$ could equally be represented by a row matrix $E[m]$, where m ranges from 0 to $WH - 1$. We transform from the row matrix representation to the two-dimensional representation by wrapping the entries of the former, just as the words on this page are wrapped to give a two-dimensional document [13]. The rows of the two dimensional signal $E[x', y']$ are placed side by side to form the one-dimensional row matrix $E[m]$.

From this point on, all signals will be considered row matrices corresponding to a two dimensional matrix by means of wrapping. Furthermore, the elements of the matrix corresponding to the signal of the object as illuminated by the nth pattern will be

denoted by $E_n^{\text{obj}}[m]$ when considering that particular illumination pattern individually, as opposed to $E^{\text{obj}}[n, m]$ when all patterns are considered at once.

2.3.1. Discretization of the Continuous Result

Let $E_n^{\text{obj}}[m] = \gamma[m]S_n[m] = S_n[m]t[m]e^{i\varphi[m]}$ be the discrete representation of the electromagnetic wavefront corresponding to the object as illuminated by the nth pattern, $S_n[m] = B_n[m]e^{\mathrm{i}\psi_n[m]}$. If the object ORF $\gamma(x, y)$ is sampled on a $W \times H$ grid, to produce $\gamma[m]$, then m ranges from 0 to $N-1$, where $N = WH$; and as will become evident later, the measurement index n must range from 0 to $2N - 1$.

Suppose that we have access to the magnitude of $E_n^{\text{out}}[k] = \mathfrak{F}(\omega)\{E_n^{\text{obj}}[m]\}/\mathrm{i}\lambda f$ (eq. (2.3)). Then, a relation between the phase of a discrete signal and the magnitude of the DFT of that signal would suffice for reconstructing the signal using the method of multiplexing. We will give this relationship here, with the proof delegated to appendix A.3.

Theorem 2.3.1. *Let $f[n] = A[n]e^{\mathrm{i}\theta[n]}$ be a discrete complex signal of length N, with $A[n] = |f[n]|$. Assume that all arguments of f are taken modulo N, such that $f[n-1] = f[(n-1) \mod N]$. Then, the backward phase difference at each point of the signal relates to the magnitude of its discrete Fourier transform (DFT) as*

$$\frac{1}{N}\sum_{\omega=0}^{N-1}\left|\hat{f}[\omega]\right|^2 e^{-2\pi\mathrm{i}\omega/N} = \sum_{n=0}^{N-1}|f[n]||f[n-1]|e^{-\mathrm{i}\nabla\theta[n]}, \tag{2.28}$$

where $\nabla\theta[n] \coloneqq \theta[n] - \theta[n-1]$ is introduced for the backward difference, and the hat denotes the DFT.

With theorem 2.3.1 we have a relation between the gradient of a signal, the magnitude of the signal, and the magnitude of its DFT. The magnitude of the signal is assumed obtainable through intensity measurements. Similarly, the magnitude of the DFT is assumed obtainable through intensity measurements and eq. (2.3).

The power spectral centroid for a certain signal $f[m]$ of N samples is given by

$$\Omega = -\frac{N}{2\pi}\arg\left(\sum_{\omega=0}^{N-1}\left|\hat{f}[\omega]\right|^2 e^{-2\pi\mathrm{i}\omega/N}\right), \tag{2.29}$$

where the hat denotes the DFT. Here, m and ω are integers that range from 0 to $N-1$. This expression is equivalent to that given in eq. (2.15), when either dimension of the latter is considered separately (either u or v). This is most easily seen by considering what each expression calculates: the discrete expression sums N phasors spread in angle

uniformly around the unit circle, but with lengths corresponding to the power of the nth frequency component of the signal. The angle of the resulting vector in the complex plane then corresponds to the centroid of the power spectrum, as is illustrated in fig. 2.5. Likewise, eq. (2.15) integrates over all frequencies weighted by their power as present in the signal. Both expressions correspond to the same quantity, and when considering a signal that vanishes at infinity and is sampled below the Nyquist frequency, they are exactly equal. This then implies that the discrete expression given by eq. (2.29) should converge to the continuous expression given by eq. (2.15); this is indeed the case, as shown in fig. 2.6.

We can substitute E_n^{obj} for f in theorem 2.3.1 and use eq. (2.3) to get a totally discrete analog to the continuous main result (eq. (2.14))

$$\boxed{\frac{\lambda^2 f^2}{N}\sum_{k=0}^{N-1}\left|E_n^{\text{out}}[k]\right|^2 e^{-2\pi ik/N} = \sum_{m=0}^{N-1}\left|E_n^{\text{obj}}[m]\right|\left|E_n^{\text{obj}}[m-1]\right|e^{-\mathrm{i}(\nabla\psi_n[m]+\nabla\varphi[m])},} \tag{2.30}$$

where we have used that $\omega = k/\lambda f$ [7]. Here, ∇ is the backward difference operator, the discrete analog of the gradient, and the hat denotes the DFT. Note that the exponents remain dimensionless, as they should, through the dimensionality of the grid on which the signal is sampled.

We can write eq. (2.30) in terms of the power spectral centroid (eq. (2.29))

$$\Omega = -\frac{N}{2\pi}\arg\left(\sum_{m=0}^{N-1}\left|E_n^{\text{obj}}[m]\right|\left|E_n^{\text{obj}}[m-1]\right|e^{-\mathrm{i}(\nabla\psi_n[m]+\nabla\varphi[m])}\right), \tag{2.31}$$

where we have dropped the overall scaling coefficient preceding the sum as it does not influence the arg function.

There is the apparent ambiguity regarding the phase gradient to dispel: eq. (2.30) is one-dimensional, but the phase gradient is inherently two-dimensional. The two dimensional phase gradient is obtained as follows. Calculate the phase gradient once according to eq. (2.30) to obtain the gradient across one dimension, then, rotate the matrix corresponding to the signal of interest by a quarter turn prior to wrapping and calculate the phase gradient once more to obtain the gradient across the second dimension.

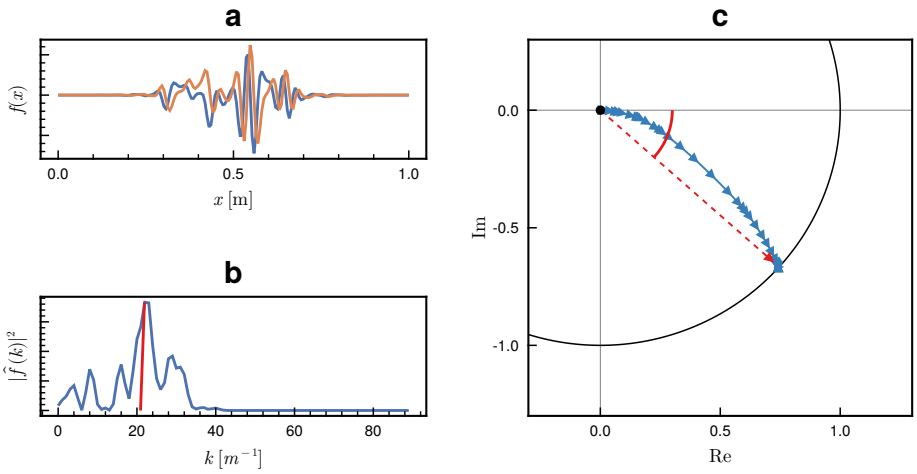

Figure 2.5.: A signal corresponding to some one-dimensional optical response function (a) is shown for its real and imaginary components, along with a graphical representation of eq. (2.29) (c). Each phasor in the sum of eq. (2.29) is drawn as a vector, head-to-tail with respect to the one preceding it in the sum. The vector drawn from the origin (dashed, red) to the last drawn vector then corresponds to the value of eq. (2.29). The angle of this vector corresponds to the power spectral centroid. The latter is also drawn on the power spectrum of the signal as a vertical red line (b).

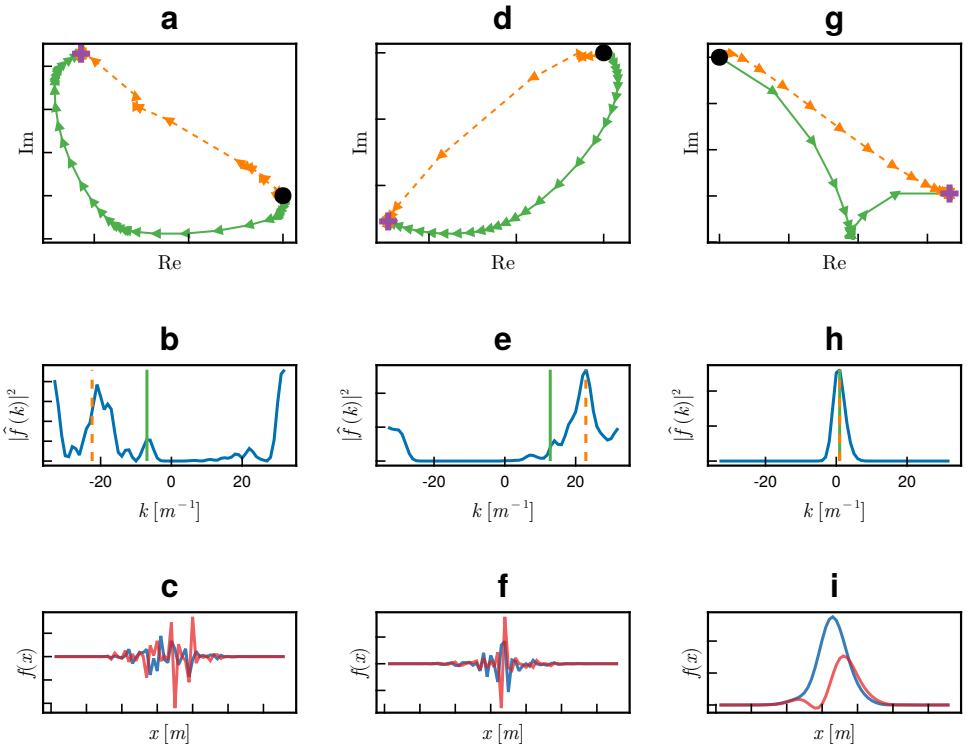

Figure 2.6.: Three one-dimensional optical response functions are shown as their real and imaginary components (c, f, i). Two signals are sampled above the Nyquist frequency (c, f), and one below (i). The power spectra (b, e, f) of the signals (c, f, i, respectively) are shown. In the power spectrum plots, the Left Hand Side (LHS) of the naive discretization of the main result (the one-dimensional equivalent of eq. (2.27)) is shown as a solid green line. The Right Hand Side (RHS) is shown as a dashed orange line; when the two meet, the equality holds. From inspection of the plotted LHS and RHS of each power spectrum, it is evident that the naive discretization only holds for signals that are sampled below the Nyquist frequency. Similarly, we show the phasors that make the sum of the LHS (solid green) and RHS (dashed orange) of the exact discrete result (eq. (2.30)). The latter is shown in (a, d, g) for the signals (c, f, i) respectively. As summing phasors entails drawing them head-to-tail, the LHS and RHS are equal when the paths that their respective phasors form converge to the same point in the complex plane. This is indeed the case for all signals, as is evident from (a, d, g), where the origin has been marked with a black circle and the point of convergence with a purple cross.

2.3.2. Matrix Form Representation

By taking multiple measurements according to eq. (2.30), we form a system of linear equations. This system is best represented in matrix form, such that the phase gradient can be separated and solved for. We will now proceed to find the matrix representation of eq. (2.30).

The Left Hand Side (LHS) and Right Hand Side (RHS) of eq. (2.30) are both phasors; taking the real part of each and using the identity $\cos(a+b) = \cos(a)\cos(b) - \sin(a)\sin(b)$, we obtain

$$\begin{aligned}\frac{\lambda^2 f^2}{N}\sum_{k=0}^{N-1}\left|E_n^{\text{out}}[k]\right|^2\cos(2\pi k/N) = \\ \sum_{m=0}^{N-1}\left|E_n^{\text{obj}}[m]\right|\left|E_n^{\text{obj}}[m-1]\right| \times (\cos(\nabla\psi_n[m])\cos(\nabla\varphi[m]) \\ -\sin(\nabla\psi_n[m])\sin(\nabla\varphi[m])).\end{aligned} \tag{2.32}$$

This equation can already be represented in matrix form, but it is handy to first label the longer terms. Let the LHS, the measurable quantity, be given by

$$\eta_n = \frac{\lambda^2 f^2}{N}\sum_{k=0}^{N-1}\left|E_n^{\text{out}}[k]\right|^2\cos\left(2\pi k/N\right). \tag{2.33}$$

Two additional quantities are defined to represent the RHS of eq. (2.32)

$$\begin{Bmatrix}\Gamma_n^c[m]\\ \Gamma_n^s[m]\end{Bmatrix} = \left|E_n^{\text{obj}}[m]\right|\left|E_n^{\text{obj}}[m-1]\right|\begin{Bmatrix}\cos(\nabla\psi_n[m])\\ -\sin(\nabla\psi_n[m])\end{Bmatrix}, \tag{2.34}$$

after which it can be written as a row matrix with the terms related to φ factored out

$$\Gamma_n[m] = \begin{pmatrix}\Gamma_n^c[m] & \Gamma_n^s[m]\end{pmatrix}. \tag{2.35}$$

Lastly, the terms related to the phase φ are grouped together as a column matrix for convenience

$$\theta[m] = \begin{pmatrix}\theta^c[m]\\ \theta^s[m]\end{pmatrix} = \begin{pmatrix}\cos(\Delta\varphi[m])\\ \sin(\Delta\varphi[m])\end{pmatrix}, \tag{2.36}$$

such that the entire right hand side of eq. (2.32) can be written as $\sum_{m=0}^{N-1}\Gamma_n[m]\theta[m]$. If all $2N$ measurements are taken into consideration, then the right hand side of eq. (2.32)

may be represented graphically by a table where the entries in the nth row represent the nth measurement

$$\underbrace{\left.\begin{array}{|c|c|c|c|c|c|}\hline \Gamma_1^c[1]\cdot\theta^c[1] & \dots & \Gamma_1^c[N]\cdot\theta^c[N] & \Gamma_1^s[1]\cdot\theta^s[1] & \dots & \Gamma_1^s[N]\cdot\theta^s[N] \\ \hline \vdots & \ddots & \vdots & \vdots & \ddots & \vdots \\ \hline \Gamma_{2N}^c[1]\cdot\theta^c[1] & \dots & \Gamma_{2N}^c[N]\cdot\theta^c[N] & \Gamma_{2N}^s[1]\cdot\theta^s[1] & \dots & \Gamma_{2N}^s[N]\cdot\theta^s[N] \\ \hline \end{array}\right\}2N}_{2N}$$

This forms the last definition, and with that we can write eq. (2.32) much more compactly as

$$\eta_n = \sum_{m=0}^{N-1} \Gamma_n[m]\theta[m]. \tag{2.37}$$

The phase gradient (backward difference) of the object signal is then recovered from intensity measurements by solving for θ, and with the relation

$$\nabla\varphi[m] = \arg(\theta^c[m] + \mathrm{i}\theta^s[m]). \tag{2.38}$$

The system of equations is now best summarized in matrix notation,

$$\boldsymbol{\Gamma\theta} = \boldsymbol{\eta}, \tag{2.39}$$

where $\boldsymbol{\eta}$ is a vector of length $2N$ related to the centroid position with entries given by eq. (2.33), $\boldsymbol{\theta}$ is a vector of length $2N$ related to the phase gradient with entries given by eq. (2.36), and $\boldsymbol{\Gamma}$ is a square matrix with entries determined by the magnitude of the object signal and the illumination patterns according to eq. (2.35), in the fashion described in section 2.2.1.

2.3.3. Numerical Simulation of Phase Reconstruction

It is now of interest to invert eq. (2.39) in order to solve for $\boldsymbol{\theta}$. After which the phase gradient can be recovered using eq. (2.38). The phase $\varphi(x, y)$ is reconstructed by numerically integrating the phase gradient.

Since we ultimately need to invert eq. (2.39) in order to reconstruct the phase, it must be so that $\mathbf{\Gamma}$ is full-rank, or alternatively that the determinant of $\mathbf{\Gamma}$ is non-vanishing [14, 1]. The matrix $\mathbf{\Gamma}$ is entirely determined by the illumination patterns, so this is the key guiding principle in choosing them. To solve the linear system of equations given by eq. (2.39) one must have at least $2N$ equations for the $2N$ unknowns, therefore $2N$ measurements must be taken. However, use of compressive sampling significantly lowers the required number of measurements [12].

We simulated the reconstruction of a complex signal E^{obj} according to the proposed method by writing a computer program that first constructs the signal, then deletes the phase information, and finally reconstructs the complex signal from intensity information alone. The algorithm used in this program is given in algorithm 1.

Algorithm 1 Simulation of the recovery of the phase of a complex signal, represented as the $W \times H$ matrix E (of $N = WH$ elements) through real-valued "measurements".

$E \leftarrow$ a $W \times H$ complex matrix ▷ Only $|E|$ is assumed known.
$S \leftarrow$ array of $2N$ uniformly distributed complex random arrays of length $2N$
$\Psi \leftarrow \arg(S)$ ▷ The phase of the elements of S.
$f_x \leftarrow E$, flattened
$E_{\text{rot}} \leftarrow E$ rotated by 90 degrees ▷ E_{rot} is then $H \times W$.
$f_y \leftarrow E_{\text{rot}}$, flattened

Let $\beta[n,m] = |S[n][m]| \times |S[n][m-1]| \times |E[m]| \times |E[m-1]|$. Also let $\alpha_c[n,m] = \cos(\Psi[n][m]) - \cos(\Psi[n][m-1])$, and let $\alpha_s[n,m]$ be defined similarly but with the sine function substituted for the cosine function. The reconstruction matrix Γ can now be formed. It will consist only of measurable quantities.

$$\Gamma \leftarrow \underbrace{\left.\begin{array}{|c|c|c|c|c|c|}\hline (\beta\cdot\alpha_c)[1,1] & \dots & (\beta\cdot\alpha_c)[1,N] & -(\beta\cdot\alpha_s)[1,1] & \dots & -(\beta\cdot\alpha_s)[1,N] \\ \hline \vdots & \ddots & \vdots & \vdots & \ddots & \vdots \\ \hline (\beta\cdot\alpha_c)[2N,1] & \dots & (\beta\cdot\alpha_c)[2N,N] & -(\beta\cdot\alpha_s)[2N,1] & \dots & -(\beta\cdot\alpha_s)[2N,N] \\ \hline \end{array}\right\}2N}_{2N}$$

Let $f \odot g$ denote the element-wise multiplication of the two arrays f and g, and let $\mathfrak{F}\{.\}$ denote the discrete Fourier transform. Let the signal as modulated by the nth pattern at the detector be given by $E^{\text{out}}[n] = \mathfrak{F}\{f_i \odot S[n]\}$. The measurements can now be taken and stored in η_i, where i stands for either x or y.

$$\eta_i \leftarrow \left.\begin{array}{|c|}\hline \sum_{k=1}^{N} \cos(2\pi(k-1)/N)\,|E^{\text{out}}[1][k]|^2/N \\ \hline \vdots \\ \hline \sum_{k=1}^{N} \cos(2\pi(k-1)/N)\,|E^{\text{out}}[2N][k]|^2/N \\ \hline \end{array}\right\}2N$$

$\theta_i \leftarrow \Gamma^{-1}\eta_i$
$\nabla_i \arg(E) \leftarrow \arg(\theta_i[1\dots N] + \mathrm{i}\theta_i[N+1\dots 2N])$

At this point, the phase gradients $\nabla_i \arg(E)$, where i stands for either x or y, should be wrapped as to produce two $W \times H$ matrices. The phase of E is recovered by numerical integration of the phase gradients.

2.4. Scheme for Reconstructing Phase from Measurements

The purpose of this section is twofold. First, many topics have been discussed and it would do good to summarize. And second, we aim to give the experimenter a clear overview of what they must do in order to reconstruct the phase of a field from the intensity measurements they have taken. While we have shown how to simulate the results numerically in section 2.3, we emphasize that the measurements that an experimenter would take are not equal to the input of the algorithms described. Only the assumptions about what constitutes a known or measurable quantity are kept. Hence, this section.

If one wishes to reconstruct the phase $\varphi(x, y)$ of the ORF of an object $\gamma(x, y) = te^{\mathrm{i}\varphi(x,y)}$ corresponding to a pure phase object, where t is a real constant that takes a value between 0 and 1, then a sequence of power spectral centroid measurements $\mathbf{\Omega}_n$ must be taken, each using a different illumination pattern. Say the object ORF $\gamma(x, y)$ is assumed to be uniformly sampled on a $W \times H$ grid. Then, $N = WH$ power spectral centroid measurements $\mathbf{\Omega}_n$ are needed to reconstruct $\varphi(x, y)$. The amplitude of the object ORF t need not be known. The procedure is detailed in algorithm 2.

But if one instead wishes to reconstruct the amplitude $t(x, y)$ of the ORF of some object $\gamma(x, y) = t(x, y)e^{\mathrm{i}\varphi(x,y)}$, where $t(x, y)$ ranges from 0 to 1, then a sequence of power measurements P_n must be taken, each using a different illumination pattern. Say the object ORF $\gamma(x, y)$ is assumed to be uniformly sampled on a $W \times H$ grid. Then, $N = WH$ power measurements at the image plane are needed to reconstruct $t(x, y)$. The procedure is detailed in algorithm 3.

Lastly, if one wishes to reconstruct the phase $\varphi(x, y)$ of the ORF of some object $\gamma(x, y) = t(x, y)e^{\mathrm{i}\varphi(x,y)}$, then a sequence of power spectral centroid measurements $\mathbf{\Omega}_n$ and power measurements P_n must be taken, each using a different illumination pattern. Say the object ORF $\gamma(x, y)$ is assumed to be uniformly sampled on a $W \times H$ grid. Then, $N = WH$ measurements are needed to reconstruct $\varphi(x, y)$. The amplitude $t(x, y)$ must also be known; one can obtain it using algorithm 3. The procedure is detailed in algorithm 4.

Algorithm 2 An algorithm with which one can reconstruct the phase $\varphi(x, y)$ of the ORF of some object $\gamma(x, y) = te^{\mathrm{i}\varphi(x,y)}$, assumed to be uniformly sampled on a $W \times H$ grid, from $N = WH$ measurements of the power spectral centroid $\mathbf{\Omega}_n$. The constant amplitude t need not be known.

Input: $\Omega_u \leftarrow N$ measurements of the u component of the power spectral centroid ▷ One measurement per pattern.

Input: $\Omega_v \leftarrow N$ measurements of the v component of the power spectral centroid

Input: $D \leftarrow$ array of N complex $W \times H$ matrices ▷ The nth element of D represents the uniformly sampled illumination pattern $S_n(x, y) = B_n(x, y)e^{\mathrm{i}\psi_n(x,y)}$.

$S \leftarrow$ array with as elements the flattened elements of D

$S_{\mathrm{rot}} \leftarrow$ array with as elements the flattened elements of D, that have been rotated by 90 degrees prior to flattening

Let the total power of the nth illumination pattern be given by $P[n] = \sum_{m=1}^{N} |S[n][m]|^2$.

$$\Gamma \leftarrow \underbrace{\left.\begin{array}{|c|c|c|}\hline \frac{\lambda f}{2\pi NP[1]}|S[1][1]|^2 & \dots & \frac{\lambda f}{2\pi NP[1]}|S[1][N]|^2 \\ \hline \vdots & \ddots & \vdots \\ \hline \frac{\lambda f}{2\pi NP[N]}|S[N][1]|^2 & \dots & \frac{\lambda f}{2\pi NP[N]}|S[N][N]|^2 \\ \hline \end{array}\right\}N}_{N}$$

Let $\nabla\Psi[n]$ be the flattened gradient of the phase of the nth pattern $D[n]$, obtainable through various implementations (for example, Numpy). When calculating $\nabla\Psi[n]$, take care to account for phase wrapping. Alternatively, use theorem A.1.1 to avoid having to directly interact with the phase.

Let the x component of the nth corrective constant be given by $C_x[n] = \frac{\lambda f}{2\pi NP[n]} \sum_{m=1}^{N} |S[n][m]|^2 \nabla\Psi[n][m]$. Also let $C_y[n]$ be similarly defined with S_{rot} substituted for S.

$\nabla\varphi_x \leftarrow \Gamma^{-1}(\Omega_u - C_x)$ ▷ Or an alternative method of solving this linear system of equations.

$\nabla\varphi_y \leftarrow \Gamma^{-1}(\Omega_v - C_y)$

The phase φ is then obtained by wrapping the flattened phase gradients $\nabla\varphi_x$ and $\nabla\varphi_y$, such that the resulting matrices are of dimensions $W \times H$, and then numerically integrating the result.

Algorithm 3 An algorithm with which one can reconstruct the amplitude $t(x, y)$ of the ORF of some object $\gamma(x, y) = t(x, y)e^{\mathrm{i}\varphi(x,y)}$, assumed to be uniformly sampled on a $W \times H$ grid, from $N = WH$ single-pixel power measurements P_n.

Input: $P \leftarrow N$ measurements of the field power (integrated intensity) ▷ One measurement per pattern.

Input: $D \leftarrow$ array of N complex illumination patterns, each sampled onto a $W \times H$ grid ▷ The nth element of D represents the uniformly sampled illumination pattern $S_n(x, y) = B_n(x, y)e^{\mathrm{i}\psi_n(x,y)}$.

$S \leftarrow$ array with as elements the flattened elements of D

$$\Gamma \leftarrow \underbrace{\left.\begin{array}{|c|c|c|}\hline |S[1][1]|^2 & \dots & |S[1][N]|^2 \\ \hline \vdots & \ddots & \vdots \\ \hline |S[N][1]|^2 & \dots & |S[N][N]|^2 \\ \hline \end{array}\right\}}_{N} N$$

$I \leftarrow \Gamma^{-1}P$ ▷ Or an alternative method of solving this linear system of equations.

The amplitude of the object ORF t is then obtained by wrapping I such that the resulting matrix is of dimensions $W \times H$, and taking the square root of the result.

Algorithm 4 An algorithm with which one can reconstruct the phase $\varphi(x, y)$ of the ORF of some object $\gamma(x, y) = t(x, y)e^{\mathrm{i}\varphi(x,y)}$, assumed to be uniformly sampled on a $W \times H$ grid, from $N = WH$ measurements of the power spectral centroid $\mathbf{\Omega}_n$. The amplitude $t(x, y)$ is assumed known.

Input: $P \leftarrow N$ measurements of the total power ▷ One measurement per pattern.

Input: $A \leftarrow$ the sampled amplitude $t[x, y]$, flattened to an array of length N ▷ Obtainable through algorithm 3.

Input: $\Omega_u \leftarrow N$ measurements of the u component of the power spectral centroid ▷ One measurement per pattern.

Input: $\Omega_v \leftarrow N$ measurements of the v component of the power spectral centroid

Input: $D \leftarrow$ array of N complex illumination patterns, each sampled onto a $W \times H$ grid ▷ The nth element of D represents the uniformly sampled illumination pattern $S_n(x, y) = B_n(x, y)e^{\mathrm{i}\psi_n(x,y)}$.

$S \leftarrow$ array with as elements the flattened elements of D

$S_{\mathrm{rot}} \leftarrow$ array with as elements the flattened elements of D, that have been rotated by 90 degrees prior to flattening

$$\Gamma \leftarrow \underbrace{\left.\begin{array}{|c|c|c|}\hline \frac{\lambda f}{2\pi P[1]}|A[1]S[1][1]|^2 & \dots & \frac{\lambda f}{2\pi P[1]}|A[N]S[1][N]|^2 \\ \hline \vdots & \ddots & \vdots \\ \hline \frac{\lambda f}{2\pi P[N]}|A[1]S[N][1]|^2 & \dots & \frac{\lambda f}{2\pi P[N]}|A[N]S[N][N]|^2 \\ \hline \end{array}\right\} N}_{N}$$

Let $\nabla\Psi[n]$ be the flattened gradient of the phase of the nth illumination pattern $D[n]$, obtainable through various implementations (for example, Numpy). When calculating $\nabla\Psi[n]$, take care to account for phase wrapping. Alternatively, use theorem A.1.1 to avoid having to directly interact with the phase.

Let the x component of the nth corrective measurement constant be given by $C_x[n] = \frac{\lambda f}{2\pi P[n]} \sum_{m=1}^{N} |A[m]S[n][m]|^2 \nabla\Psi[n][m]$. Also let $C_y[n]$ be similarly defined with S_{rot} substituted for S.

$\nabla\varphi_x \leftarrow \Gamma^{-1}(\Omega_u - C_x)$ ▷ Or an alternative method of solving this linear system of equations.

$\nabla\varphi_y \leftarrow \Gamma^{-1}(\Omega_v - C_y)$

The phase φ is then obtained by wrapping the flattened phase gradients $\nabla\varphi_x$ and $\nabla\varphi_y$, such that the resulting matrices are of dimensions $W \times H$, and then numerically integrating the result.

3. Results

Three separate sets of illumination patterns were used in a numerical simulation, according to algorithm 1: a set of uniform random patterns, a set of computer generated speckle patterns, and a set of speckle patterns obtained experimentally from a multimode fiber. Unless otherwise stated, the monochromatic illumination is of wavelength $\lambda = 620\,\text{nm}$, and the focal distance is $f = 100\,\text{mm}$. We show the phase gradient instead of the phase, which is trivially obtained by numerical integration, to better illustrate the accuracy of the proposed method. The ground truth phase gradient was obtained simply according to the definition of backward difference that is given in this thesis, namely $\nabla f[n] = f[n] - f[n-1]$.

3.1. Uniform Random Complex Illumination Patterns

A set of uniform random illumination patterns was generated using the standard library of Julia 1.9.1. In this case, the nth illumination pattern is given by $S_n[m] = A_n[m]e^{2\pi \mathrm{i} B_n[m]}$, where $A_n[m]$ and $B_n[m]$ are real uniform random arrays. A complex field was constructed and represented as a 64×64 matrix, and reconstructed using the proposed method; specifically, using algorithm 1. The results are presented in fig. 3.2, and the first of the patterns is shown in fig. 3.1.

The set of uniformly distributed random patterns produced a reconstruction with an error of the order of 10^{-11} in phase and 10^{-12} in amplitude. Remnants of both the phase and amplitude of the object are vaguely visible in the difference of the reconstructed phase and the ground truth (fig. 3.2 c). The amplitude reconstruction appears to produce a randomly distributed difference with respect to the ground truth (fig. 3.2 f).

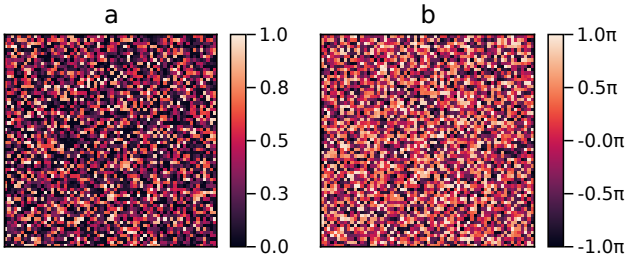

Figure 3.1.: A uniformly distributed random complex field is shown in intensity (a) and phase (b). The region of the object plane that is shown is a square of length 10 mm. This is one of the illumination patterns used in the reconstruction of fig. 3.2.

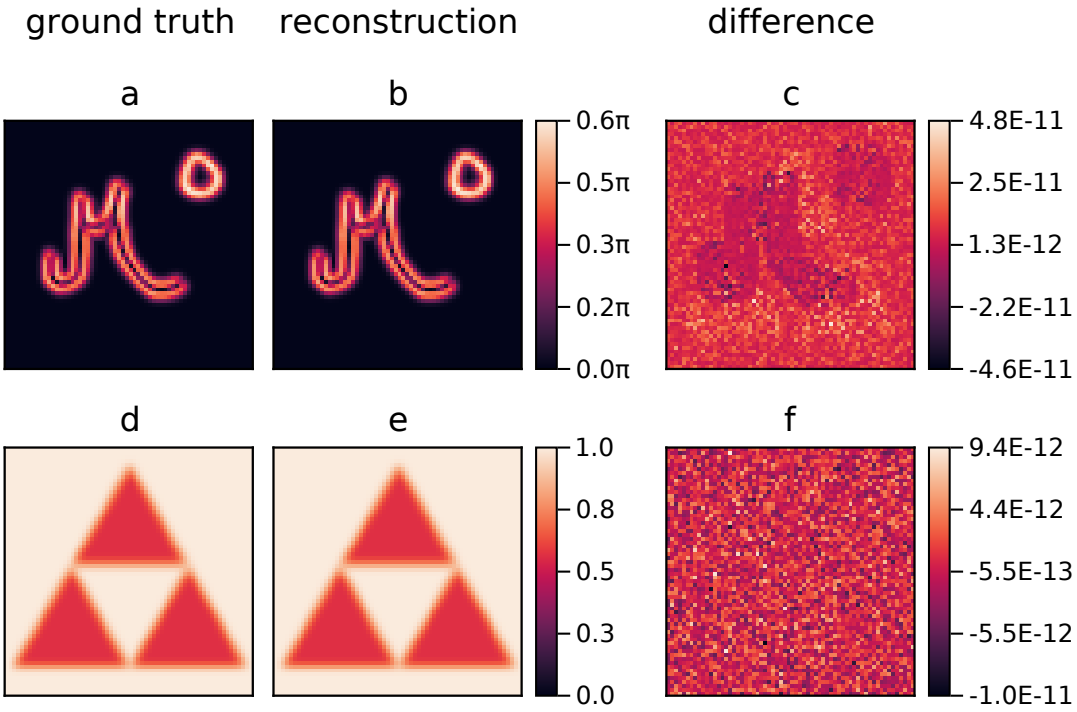

Figure 3.2.: Results of the proposed method for uniformly distributed complex random masks. The simulation input of the phase gradient (a) and intensity (d) of the object field are shown. The region of the object plane that is shown is a square of length 10 mm. Uniformly distributed random complex fields were used as illumination patterns (fig. 3.1). The reconstructed phase gradient (b) and intensity (e) are shown alongside their differences with respect to the simulation inputs (c, f). The reconstruction error is of the order of 10^{-11}; the phase and amplitude of the object field are vaguely visible in the error of the phase gradient (c), but the general pattern is otherwise random.

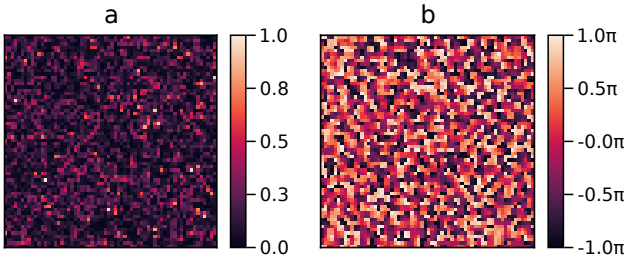

Figure 3.3.: A computer generated speckle pattern represented as a 64×64 matrix is shown in intensity (a) and phase (b). The region of the object plane that is shown is a square of length 10 mm. The pattern was generated using algorithm 5 which can be found in appendix B.1. This speckle pattern corresponds to a wavelength of $\lambda = 620\,\text{nm}$ and $NA = 0.75$. The parameters for the algorithm are $\kappa = 0.5$ and $R_{\text{cutoff}} = 24$. This is one of the illumination patterns used in the reconstruction of fig. 3.4.

3.2. Artificial Complex Speckle Illumination Patterns

A set of random patterns was additionally generated, which aimed to reproduce the speckle patterns that get produced by the scrambling of coherent light as it passes through a multi-mode waveguide [15]. The patterns were constructed according to algorithm 5, which can be found in appendix B.1. The patterns are of size 64×64, and the parameters for the algorithm were $\kappa = 0.5$ and $R_{\text{cutoff}} = 24$, which corresponds to a numerical aperture of $NA = 0.75$. One of the patterns is depicted in fig. 3.3, and the results are shown in fig. 3.4.

The reconstruction using this set of patterns resulted in what we consider to be an exact result, differing by a factor of 10^{-10} in the phase gradient from the ground truth, and a factor of 10^{-11} in amplitude (fig. 3.4 c, f). Remnants of the object phase and amplitude are somewhat visible in the error of the phase gradient (fig. 3.4 c).

3.2.1. Dependence of Reconstruction on Algorithm Parameters

In order to be able to reconstruct the field, it must be so that $\mathbf{\Gamma}$ is full-rank, or alternatively that the determinant of $\mathbf{\Gamma}$ is non-vanishing (see section 2.3.3). Since $\mathbf{\Gamma}$ is formed from the illumination patterns, it is of interest to study the effects of the parameters of algorithm 5 on the quality of the reconstruction.

We opted to keep the correlation κ set to 0.5 since that is physically representative of

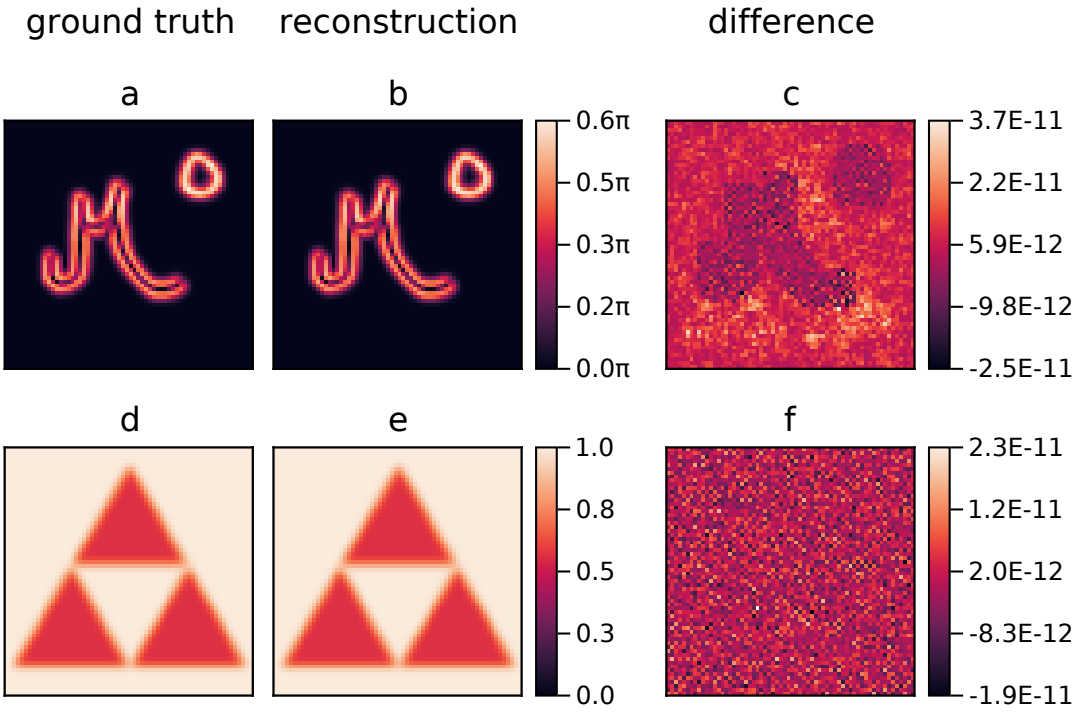

Figure 3.4.: Results of the proposed method for computer generated complex speckle patterns, generated using algorithm 5 which can be found in appendix B.1. The region of the object plane that is shown is a square of length 10 mm. The simulation input of the phase gradient (a) and intensity (d) of the object field are shown. Computer generated complex speckle patterns were used for the reconstruction (fig. 3.3). The reconstructed phase gradient (b) and intensity (e) are shown alongside their differences with respect to the simulation inputs (c, f). The reconstruction error is of the order of 10^{-11}; the phase and amplitude of the object field are vaguely visible in the error of the phase gradient (c).

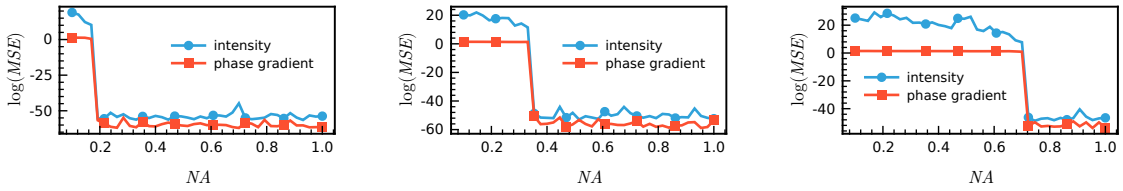

i 16×16 ii 32×32 iii 64×64

Figure 3.5.: The mean square error of the reconstruction for both phase gradient and intensity was evaluated for varying numerical aperture (NA) values. Three detectors of varying resolution are evaluated: a detector of resolution 16×16 (i), 32×32 (ii), and 64×64 (iii). For each detector there is a critical NA below which the reconstruction fails entirely.

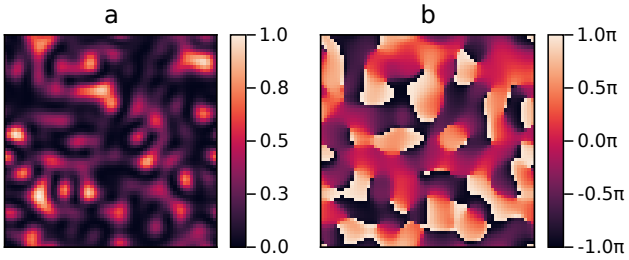

Figure 3.6.: One of the illumination patterns that form an ill-conditioned multiplexing matrix (see fig. 3.5). A computer generated speckle pattern represented as a 64×64 matrix is shown in intensity (a) and phase (b). The region of the object plane that is shown is a square of length 10 mm. The pattern was generated using algorithm 5 which can be found in appendix B.1. This speckle pattern corresponds to a wavelength of $\lambda = 620\,\text{nm}$ and $NA = 0.2$. The parameters for the algorithm are $\kappa = 0.5$ and $R_{\text{cutoff}} = 6$. This is one of the illumination patterns used in the reconstruction of fig. 3.7.

the nature of the speckle patterns created by multi-mode fibers. The mean square error of the reconstructed field was evaluated for varying numerical aperture (NA) values. The same field was used as in the rest of the simulations, but sampled on a grid of size 64×64, one of size 32×32, and another of size 16×16, to illustrate the relation of the sampling grid to the reconstruction quality. The results are presented in fig. 3.5.

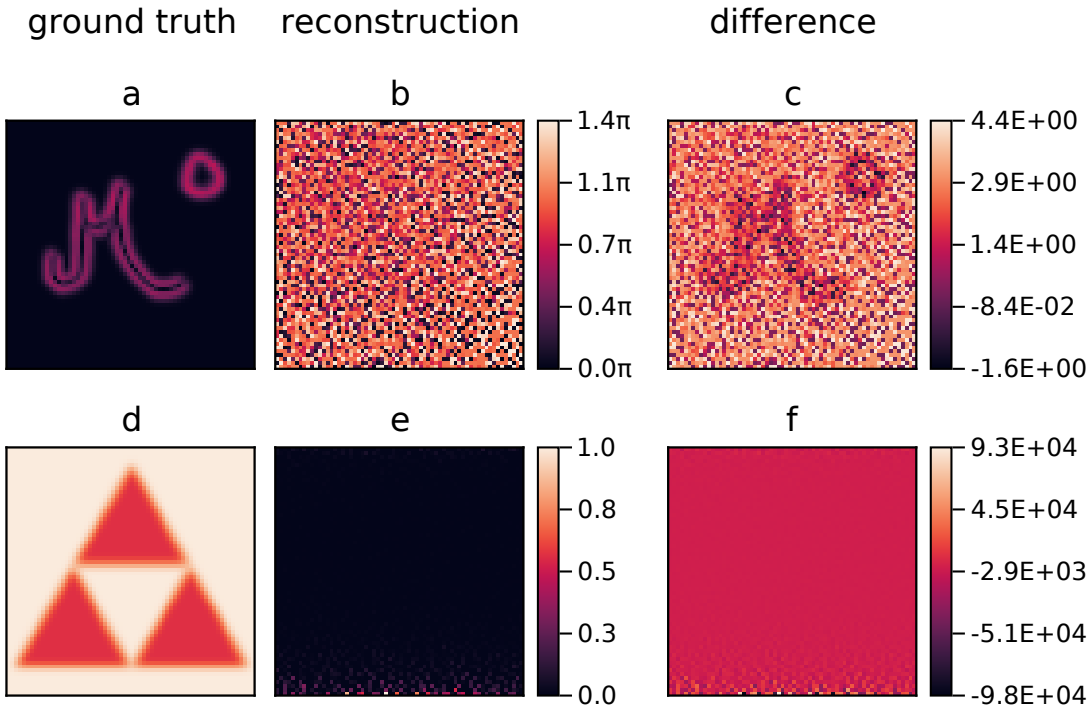

Figure 3.7.: The result of using illumination patterns that form an ill-conditioned multiplexing matrix (see fig. 3.5). The region of the object plane that is shown is a square of length 10 mm. The simulation input of the phase gradient (a) and intensity (d) of the object field. Computer generated complex speckle patterns of low NA were used for the reconstruction (fig. 3.6). The reconstructed phase gradient (b) and intensity (e) are shown alongside their differences with respect to the simulation inputs (c, f). The intensity (d, e) is normalized individually with respect to the ground truth and reconstruction. The reconstruction fails entirely due to the ill-conditioned multiplexing matrix.

3.3. Comparison with Previous Approach

In order to demonstrate the added value of the non-trivial discrete representation derived in section 2.3, we show the results of our implementation of the theory described in [11]. The field to reconstruct was kept identical to that used in the proposed method. We remind the reader that the method described in [11] uses binary illumination patterns. Since this method solves for the phase gradient, as opposed to the backward difference, we compute the ground truth using Numpy's gradient function. The results are presented in fig. 3.9, and one of the illumination patterns is shown in fig. 3.8.

We stress that the authors did not provide a method for numerical simulation of their results, so we opted for the naive implementation of the theory that they present. Specifically, we replace Fourier transforms with discrete Fourier transforms, and integrals with sums. As mentioned in section 2.2.4, our proposed method is identical to the method derived in [11] for those special cases that are considered there; namely, real valued illumination patterns, and real valued illumination of pure phase objects. Therefore, a naive implementation of our theory would produce identical results to the results described here. The purpose of this comparison is only to demonstrate the added value of the discrete representation derived in section 2.3.

By inspection of the difference between the reconstruction and the ground truth alone, we see that the reconstruction is not exact (fig. 3.9 c, f). The inputs are clearly visible in the differences, and the differences are of the order of 10^{-1}. The proposed method clearly improves upon this, with a difference between reconstruction and ground truth of the order of 10^{-11}.

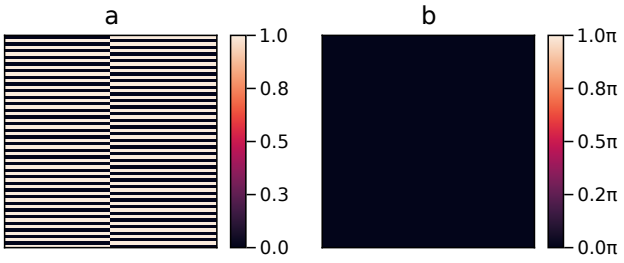

Figure 3.8.: Binary illumination patterns were obtained from the shifted and rescaled Walsh-Hadamard functions [11]. The intensity (a) is shown, but the phase (b) is of course constant. The region of the object plane that is shown is a square of length 10 mm. This is one of the illumination patterns used in the reconstruction of fig. 3.9.

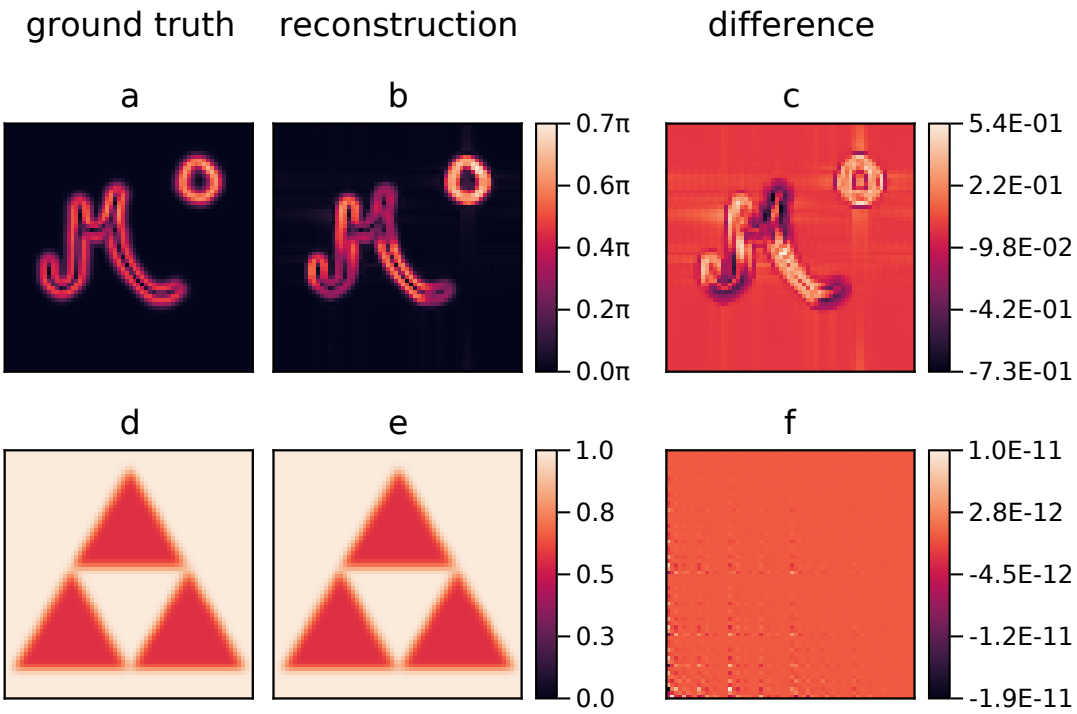

Figure 3.9.: Results of our naive implementation of the method described in [11]. The simulation input of the phase gradient (a) and intensity (d) of the object field were represented as a complex 64×64 matrix. The binary illumination patterns are obtained from the shifted and rescaled Walsh-Hadamard functions, of which one is depicted in fig. 3.8 [11]. The region of the object plane that is shown is a square of length 10 mm. The reconstructed phase gradient (b) and intensity (e) are shown alongside their differences with respect to the simulation inputs (c, f). The reconstruction error is of the order of 10^{-1}; the input is clearly visible in the error. The proposed method results in a reconstruction error ten orders of magnitude smaller than the method described in [11].

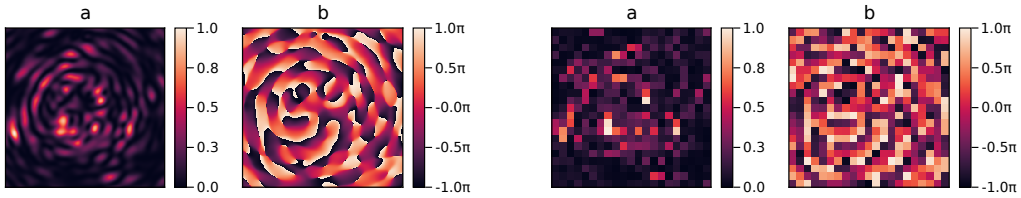

i Experimentally obtained speckle pattern

ii Downsampled speckle pattern

Figure 3.10.: An experimentally obtained speckle pattern of a multi-mode fiber is shown in intensity (a) and phase (b). This one of the illumination patterns used in the reconstruction of fig. 3.11. The obtained pattern (i) was downsampled (ii) because we had access to but 900 patterns, and the reconstruction requires $2N$ patterns if N is the total number of resolution elements. The region of the downsampled object plane that is shown is a square of length 10 mm.

3.4. Experimentally Obtained Complex Speckle Illumination Patterns

Lastly, 900 measurements were taken of the complex field that was emitted by a multi-mode fiber, experimentally. These measurements were then used as the illumination patterns in the simulation. One of the patterns is depicted in fig. 3.10. The monochromatic illumination is of wavelength $\lambda = 640\,\text{nm}$, and the focal distance is taken to be $f = 100\,\text{mm}$.

If the field to reconstruct is represented as a $W \times H$ matrix, then the numerical simulation requires $2WH$ unique speckle patterns. Therefore it was necessary to downsample both the object and the masks prior to simulation to the size 21×21. This set of patterns produce a similar result to the computer generated speckle patterns; the result is presented in fig. 3.11.

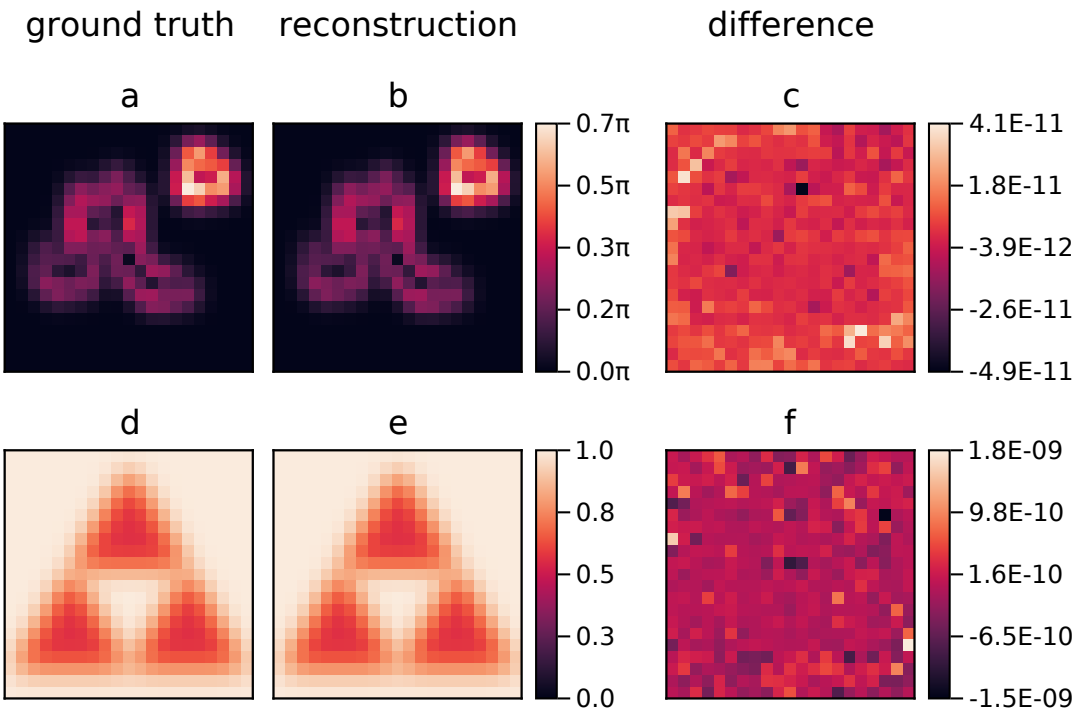

Figure 3.11.: Results of the proposed method for complex speckle patterns, obtained experimentally. The simulation input of the phase gradient (a) and intensity (d) of the object field are shown. The region of the object plane that is shown is a square of length 10 mm. Speckle patterns as obtained experimentally from a multi-mode fiber, then digitally downsampled, were used for the illumination patterns (fig. 3.10). The image size is relatively small because we had access to but 900 patterns. The reconstructed phase gradient (b) and intensity (e) are shown alongside their differences with respect to the simulation inputs (c, f). The errors (c, f) are of order 10^{-11} and appear to be mostly random; the phase of the object field is vaguely visible in the difference of the phase and the ground truth (c).

4. Discussion

We have shown that it is possible to exactly reconstruct a complex field by measuring only the intensity and centroid position of the magnitude of its Fourier transform. The method works by means of multiplexing; the key idea is to choose the multiplexing weights according to a set of pre-determined complex patterns.

The proposed method is equivalent to solving a linear system of equations of, say, N unknowns, where N increases with the resolution of the reconstruction. Therefore, N measurements are required to make the system of equations solvable. We emphasize that use of compressive sampling significantly lowers the required number of measurements [12].

A recent paper demonstrates that it is possible to recover a complex signal exactly from the magnitude of its inner products with a set of so called sensing vectors [16]. The paper concludes by suggesting possible future research directions, one of which being to study the case when the set of sensing vectors is more structured than what the authors considered. This thesis demonstrates exactly this, with the set of sensing vectors being the set of complex illumination patterns used to form the multiplexing weights. A set of structured random sensing vectors is explicitly mentioned as being highly interesting for the authors; the set that was used in this thesis is indeed that, random speckle patterns as produced by a multi-mode fiber.

More work still can be done in improving and understanding the proposed method. A study of the effect of detector noise on the reconstruction of the field is of great significance. The proposed method requires knowledge of the illumination patterns, therefore it is of interest to study systems that can generate complex fields in a deterministic way.

Although experimental work was considered outside of the scope of this thesis, the theoretical results turned out to be promising. As a result, we are currently planning experiments to test the derived results. The experiments will make use of a multi-mode fiber for the illumination patterns.

5. Conclusion

A scheme for recovering a complex signal from intensity measurements was devised which uses a series of complex-valued weighting patterns to sample the signal at different points simultaneously. The measurements are then solved for the values at each point individually by demultiplexing the measurements. The complex signal is recovered both in phase and amplitude up to a difference of the order of 10^{-11} with respect to the ground truth.

A continuous equation relating the phase of a complex signal to its Fourier magnitude is derived, along with a discrete analog ideal for computer simulations. Proofs are provided to motivate the scheme, and the algorithms used in the simulations are provided as well.

The phase reconstruction scheme was shown to work best for uniformly distributed random weights. Speckle patterns as produced by a waveguide are then used for the multiplexing weighting scheme, with equally satisfactory results. The conditions under which the scheme will or will not work are discussed as well.

6. Acknowledgements

During the entire length of time that I worked on this project, it was not once the case that my supervisor, dr. Ksenia Abrashitova, was not available to answer my questions. At numerous times I had gotten myself confused with subtleties, and many times over it was the case that dr. Abrashitova sat with me, for the greater part of the day, in order to look for a solution.

Although my appointed daily supervisor was dr. Abrashitova, it was always the case that dr. Lyuba Amitonova was available to discuss my work. The feedback that dr. Abrashitova and dr. Amitonova gave was of high quality and served to push me and the project forward. I attribute the quality of the result to this aspect in particular.

When I had thoughts to discuss, as I did throughout the beginning of my process, dr. Tristan van Leeuwen has heard those thoughts and helped make them concrete and concise.

Lastly, I would like to thank Mara van der Meulen for proof reading this thesis multiple times, and for her assistance with some proofs.

6.1. Software and Tooling

The numerical simulations were implemented in Julia 1.9.1. All plots were created using Makie [17].

7. Bibliography

[1] D. C. Ghiglia, Binary multiplexing and the phase-retrieval problem, *Opt. Lett.* **7**, 602 (1982).

[2] K. Jaganathan, Y. C. Eldar B. Hassibi, Phase retrieval: An overview of recent developments (2015).

[3] A. Patterson, A fourier series method for the determination of the components of interatomic distances in crystals, *Physical review* **46**, 372 (1934).

[4] A. Patterson, Ambiguities in the x-ray analysis of crystal structures, *Physical review* **65**, 195 (1944).

[5] A. Walther, The question of phase retrieval in optics, *Optica acta* **10**, 41 (1963).

[6] R. HANBURY BROWN R. Q. TWISS, A test of a new type of stellar interferometer on sirius, *Nature* **178**, 1046 (1956).

[7] J. W. J. W. Goodman, *Introduction to Fourier optics*, McGraw-Hill physical and quantum electronics series. (NL-LeOCL)841781133 (McGraw-Hill, San Francisco, 1968).

[8] J. R. Fienup, Reconstruction of an object from the modulus of its fourier transform, *Opt. Lett.* **3**, 27 (1978).

[9] R. G. Lane, Blind deconvolution of speckle images, *J. Opt. Soc. Am. A* **9**, 1508 (1992).

[10] R. Horisaki, R. Egami J. Tanida, Single-shot phase imaging with randomized light (spiral), *Opt. Express* **24**, 3765 (2016).

[11] F. Soldevila, V. Durán, P. Clemente, J. Lancis E. Tajahuerce, Phase imaging by spatial wavefront sampling, *Optica* **5**, 164 (2018).

[12] M. F. Duarte *et al.*, Single-pixel imaging via compressive sampling, *IEEE Signal Processing Magazine* **25**, 83 (2008).

[13] P. Gottlieb, A television scanning scheme for a detector-noise-limited system, *IEEE Transactions on Information Theory* **14**, 428 (1968).

[14] J. A. Decker M. O. Harwitt, Sequential encoding with multislit spectrometers, *Appl. Opt.* **7**, 2205 (1968).

[15] J. W. J. W. Goodman, *Statistical optics*, Wiley classics library (Wiley, New York [etc, 2000).

[16] E. J. Candes, T. Strohmer V. Voroninski, Phaselift: Exact and stable signal recovery from magnitude measurements via convex programming (2011).

[17] S. Danisch J. Krumbiegel, Makie.jl: Flexible high-performance data visualization for Julia, *Journal of Open Source Software* **6**, 3349 (2021).

A. Proofs

A.1. Fourier Transform Theorems

Some theorems regarding the Fourier transform (FT) are used in the derivations in this thesis; they are presented here with proofs. The Fourier transform of a function $f(t)$ is written as $\hat{f}(\omega) = \mathfrak{F}\{f(t)\}$ and is defined by

$$\mathfrak{F}\{f(t)\}(\omega) \coloneqq \int_{-\infty}^{\infty} f(t)e^{-2\pi \mathrm{i}\omega t}\,dt, \quad t, \omega \in \mathbb{R}^n. \tag{A.1}$$

The inverse Fourier transform is given by

$$f(t) = \int_{-\infty}^{\infty} \hat{f}(\omega)e^{2\pi \mathrm{i}\omega t}\,d\omega, \quad t, \omega \in \mathbb{R}^n. \tag{A.2}$$

Theorem A.1.1. *If a complex analytic signal $f(t)$ vanishes at infinity, then*

$$\mathfrak{F}\{\frac{d^n}{dt^n}f(t)\}(\omega) = (2\pi \mathrm{i}\omega)^n \mathfrak{F}\{f(t)\}(\omega), \quad t, \omega \in \mathbb{R}^n, \tag{A.3}$$

where $\mathfrak{F}\{.\}$ denotes the Fourier transform.

Proof. By recursively applying integration by parts, we get that

$$\begin{aligned}
\mathfrak{F}\{\frac{d^n}{dt^n}f(t)\}(\omega) &= \int_{-\infty}^{\infty} \frac{d^n}{dt^n}f(t)e^{-2\pi \mathrm{i}\omega t}\,dt && \text{(A.4)}\\
&= \sum_{k=0}^{n-1} \left[(-1)^k(-2\pi \mathrm{i}\omega)^{n-k}e^{-2\pi \mathrm{i}\omega t}\frac{d^k}{dt^k}f(t)\right]_{t=-\infty}^{t=\infty} && \text{(A.5)}\\
&\quad + (-1)^n \int_{-\infty}^{\infty} (-2\pi \mathrm{i}\omega)^n f(t)e^{-2\pi \mathrm{i}\omega t}\,dt && \text{(A.6)}\\
&= (2\pi i\omega)^n \mathfrak{F}\{f(t)\}(\omega). && \text{(A.7)}
\end{aligned}$$

The signal $f(t)$ and all of its derivatives are assumed to vanish at infinity. □

Theorem A.1.2. *If a complex analytic signal $f(t)$ vanishes at infinity, then*

$$\int f^*(t)\frac{d^n}{dt^n}f(t)dt = (2\pi i)^n \int \omega^n \left|\hat{f}(\omega)\right|^2 d\omega, \quad t, \omega \in \mathbb{R}^n. \tag{A.8}$$

Proof. For this proof we will make use of Plancherel's theorem, which we will not prove here. Taking $f_1(t)$ of Theorem 2.2.1 to be $d^n/dt^n f(t)$ and $f_2(t)$ to be $f^*(t)$ and using theorem A.1.1 we immediately obtain the result stated in the theorem. □

A.2. Derivation of Continuous Equation

Theorem 2.2.2. *If a complex analytic signal $f(t)$ vanishes at infinity, then*

$$\int |f(t)|^2 \nabla \arg(f(t))\, dt = 2\pi \int \omega \left|\hat{f}(\omega)\right|^2 d\omega, \quad t, \omega \in \mathbb{R}^n \tag{2.13}$$

where $\hat{f}(\omega)$ is the Fourier transform of $f(t)$, and $\nabla \arg(f(t))$ is the gradient of the phase of $f(t)$.

Proof. The derivative of a complex signal $f(t) = A(t)e^{\mathrm{i}\theta(t)}$ is given by

$$\dot{f}(t) = \left(\dot{A}(t) + \mathrm{i}A(t)\dot{\theta}(t)\right) e^{i\theta(t)}. \tag{A.9}$$

Integrating the quantity $f^*(t)\dot{f}(t)$ in phasor form gives

$$\int f^*(t)\dot{f}(t)\, dt = \int A(t)e^{-\mathrm{i}\theta(t)} \left(\dot{A}(t) + \mathrm{i}A(t)\dot{\theta}(t)\right) e^{\mathrm{i}\theta(t)}\, dt \tag{A.10}$$

$$= \int A(t)\dot{A}(t)\, dt + \mathrm{i} \int A(t)^2\dot{\theta}(t)\, dt \tag{A.11}$$

$$= \mathrm{i} \int A(t)^2\dot{\theta}(t)\, dt, \tag{A.12}$$

where in the last equality it was used that the first term is a perfect integral and that $f(t)$ is integrable square, from which it follows that

$$\int A(t)\dot{A}(t)\, dt = \frac{1}{2} \int \frac{d}{dt}\left[A(t)^2\right]\, dt = \frac{1}{2}\left(A(\infty)^2 - A(-\infty)^2\right) = 0. \tag{A.13}$$

Using Theorem A.1.2 in combination with eq. (A.10) yields a relation between a signal's phase gradient, its intensity, and its unnormalized mean frequency, as shown in the theorem. From inspection of the definition of the Fourier transform it is evident that the substitution of a vector of mutually independent variables for t is allowed. □

A.3. Derivation of Discrete Equation

The discrete Fourier transform (DFT) of a signal $f[n]$ is written as $\hat{f}[\omega] = \mathfrak{F}\{f[n]\}$ and is defined by

$$\mathfrak{F}\{f[n]\}(\omega) \coloneqq \sum_{n=0}^{N-1} f[n] e^{-2\pi \mathrm{i}\omega n/N}. \tag{A.14}$$

The inverse discrete Fourier transform is given by

$$f[n] = \frac{1}{N} \sum_{\omega=0}^{N-1} \hat{f}[\omega] e^{2\pi \mathrm{i}\omega n/N}. \tag{A.15}$$

Theorem 2.3.1. *Let $f[n] = A[n]e^{\mathrm{i}\theta[n]}$ be a discrete complex signal of length N, with $A[n] = |f[n]|$. Assume that all arguments of f are taken modulo N, such that $f[n-1] = f[(n-1) \mod N]$. Then, the backward phase difference at each point of the signal relates to the magnitude of its discrete Fourier transform (DFT) as*

$$\frac{1}{N} \sum_{\omega=0}^{N-1} \left| \hat{f}[\omega] \right|^2 e^{-2\pi \mathrm{i}\omega/N} = \sum_{n=0}^{N-1} |f[n]||f[n-1]| e^{-\mathrm{i}\nabla\theta[n]}, \tag{2.28}$$

where $\nabla\theta[n] \coloneqq \theta[n] - \theta[n-1]$ is introduced for the backward difference, and the hat denotes the DFT.

Proof. By substituting the inverse DFT of the signal's DFT for the signal itself, we see that

$$\sum_{n=0}^{N-1} f^*[n] f[n-1] = \sum_{n=0}^{N-1} \left(\frac{1}{N} \sum_{j=0}^{N-1} \hat{f}[j] e^{2\pi \mathrm{i} jn/N} \right)^* \left(\frac{1}{N} \sum_{k=0}^{N-1} \hat{f}[k] e^{2\pi \mathrm{i} k(n-1)/N} \right) \tag{A.16}$$

$$= \frac{1}{N} \sum_{j=0}^{N-1} \sum_{k=0}^{N-1} \hat{f}[j]^* \hat{f}[k] e^{-2\pi \mathrm{i} k/N} \frac{1}{N} \sum_{n=0}^{N-1} e^{2\pi \mathrm{i}(k-j)n/N}. \tag{A.17}$$

But for all j, k, the summand of the sum over n makes $k - j$ complete turns around the unit circle and the sum vanishes, with the exception of $j = k$, in which case the sum equals N. The equality then simplifies to

$$\sum_{n=0}^{N-1} f[n]^* f[n-1] = \frac{1}{N} \sum_{k=0}^{N-1} \left| \hat{f}[k] \right|^2 e^{-2\pi \mathrm{i} k/N}. \tag{A.18}$$

By substituting the phasor form of the signal $f[n] = A[n]e^{\mathrm{i}\theta[n]}$, with $A[n] = |f[n]|$, we obtain the result as stated in the theorem. □

B. Algorithms

B.1. Construction of Artificial Speckle Patterns

Algorithm 5 Construction of M complex speckle patterns, similar to those produced by a waveguide, of correlation κ, cut-off radius R_{cutoff}, and pattern size $N \times N$.

Require: $0 \leq \kappa \leq 1$

Require: $0 < R_{\text{cutoff}} \leq N/2$

$X \leftarrow$

1	2	…	$N-1$	N
⋮	⋮	⋮	⋮	⋮
1	2	…	$N-1$	N

$\}N$

$\underbrace{\qquad\qquad}_{N}$

$Y \leftarrow$

1	…	1
2	…	2
⋮	⋮	⋮
$N-1$	…	$N-1$
N	…	N

$\}N$

$\underbrace{\qquad\qquad}_{N}$

Let $\mathfrak{F}\{.\}$ denote the discrete Fourier transform. And let $f \odot g$ denote the element-wise multiplication of the two arrays f and g;

all other operations on arrays are to be performed element-wise as well.

$H \leftarrow (X - N/2)^2 + (Y - N/2)^2 \leq R_{\text{cutoff}}$

$U \leftarrow N \times N \times M$ array initialized with zeros

for $i \in 1 \ldots M$ **do**

$\chi \leftarrow N \times N \times 2$ uniformly distributed random array

$\chi \leftarrow 2\pi\chi - \pi$

$W \leftarrow \kappa \exp(-\mathrm{i}\chi[1 \ldots N, 1 \ldots N, 1]) + \sqrt{1-\kappa^2}\exp(-\mathrm{i}\chi[1 \ldots N, 1 \ldots N, 2])$

$U[1 \ldots N, 1 \ldots N, i] \leftarrow \mathfrak{F}^{-1}\{\text{ifftshift}\,(\text{fftshift}\,(\mathfrak{F}\{W\}) \odot H)\}$

end for

The array U now contains M complex speckle patterns of size $N \times N$.